The structure of Borneo vortices and their relationship with cold surges, the Madden–Julian oscillation and equatorial waves

Crook, J. ORCID: https://orcid.org/0000-0003-1724-1479, Hardy, S., Methven, J. ORCID: https://orcid.org/0000-0002-7636-6872, Schwendike, J., Yik, D. J. ORCID: https://orcid.org/0000-0003-1128-7425 and Yang, G.-Y. ORCID: https://orcid.org/0000-0001-7450-3477 (2025) The structure of Borneo vortices and their relationship with cold surges, the Madden–Julian oscillation and equatorial waves. Quarterly Journal of the Royal Meteorological Society, 151 (766). e4905. ISSN 0035-9009 doi: 10.1002/qj.4905 Available at https://centaur.reading.ac.uk/119641/

Received: 5 April 2024 | Revised: 15 October 2024 | Accepted: 6 November 2024

DOI: 10.1002/qj.4905

Quarterly Journal of the Royal Meteorological Society RMetS

RESEARCH ARTICLE

The structure of Borneo vortices and their relationship with cold surges, the Madden–Julian oscillation and equatorial waves

Julia Crook[1] | **Sam Hardy**[1] | **John Methven**[2] | **Juliane Schwendike**[1] | **Diong Jeong Yik**[3] | **Gui-Ying Yang**[2,4]

[1]University of Leeds, Leeds, UK

[2]University of Reading, Reading, UK

[3]Malaysian Meteorological Department, Petaling Jaya, Malaysia

[4]National Centre for Atmospheric Science, University of Reading, Reading, UK

Correspondence
Julia Crook, University of Leeds, Leeds, UK.
Email: j.a.crook@leeds.ac.uk

Funding information
Newton Fund Weather and Climate Science for Service Partnershi

Abstract

The Borneo vortex (BV) is a synoptic-scale vorticity feature found in the South China Sea near Borneo during extended Boreal winter, which can bring heavy rain to the region. Predicting this rainfall is difficult. Therefore, a better understanding of the structure of these vortices and their interaction with equatorial waves could aid forecasters. Here we divide the BVs found from 41-years of October–March ERA5 data into five clusters based on their tracks identified using relative vorticity maxima. These clusters capture distinct phenomena: vortices moving westwards across the South China Sea, vortices tracking along the north and northwest sides of Borneo, vortices sitting on the west side of Borneo, and vortices that initiate on the northwest side of Borneo, cross the equator and track eastwards along the south coast of Borneo. These clusters have a strong seasonal dependence related to the strength and southward propagation of the northeasterly flow and therefore cold-surge type. The Madden–Julian oscillation (MJO) is considerably less important than the cold surge for modulating vortex frequency but has a similar order of magnitude impact on vortex rainfall. Kelvin waves strongly modulate rainfall from all BVs. Westward-moving mixed Rossby–gravity (WMRG) and Rossby $n = 1$ (R1) waves modify frequency, rainfall, and vorticity through modification of environmental vorticity and northeasterly flow. These properties are highest when the BV is within or on the leading edge of the positive vorticity phase of R1 waves (in the northern hemisphere) or WMRG waves. Westward-moving vortices north of 4° N are often embedded in and move with R1 or WMRG waves. Examining case studies in detail, we find BVs typically extend upward to 500–400 hPa but can reach to 300 hPa, and those near the equator may not always have closed streamlines. Under vertical wind shear they may tilt, usually to the west.

KEYWORDS

atmosphere, convection, dynamics, observational data analysis, severe weather, synoptic, tropics

1 | INTRODUCTION

The heaviest rainfall over Borneo, Sumatra and Malaysia occurs during Boreal winter (December to February [DJF]), although rainfall along coastlines in this region exhibits a seasonal migration from the north (15°–20° N) in October to south of the equator in December to February (Chen et al., 2015). As a result of the intense rain, a large amount of latent heat is released which can impact global circulations and therefore the climate (Chang et al., 2005; Johnson & Houze, 1987; Lim & Chang, 1981). During DJF, the climatological winds are northeasterly north of the equator but turn to westerly south of the equator (Johnson & Houze, 1987) with a trough close to the equator. Also, during this time there are frequent cold-air outbreaks from continental China southwards over the South China Sea, driven by the Siberian high moving south, producing what is known as 'cold surge' events (Chang et al., 1979; Chang & Lau, 1980). Such events enhance the northeasterly flow in the South China Sea. These surges are moistened and warmed by their passage over tropical sea and heavy rainfall is frequently observed when cold-surge events occur (Lim et al., 2017). The northeasterly winds in the South China Sea and the westerlies just south of the equator result in a background anticlockwise (positive) vorticity in the vicinity of Borneo. Perturbations in this background vorticity often amplify into quasi-stationary anticlockwise circulation systems of the order of 500 km across (synoptic scale) usually referred to as Borneo vortices (BVs; Chang et al., 2005; Johnson & Houze, 1987; Lim & Chang, 1981). BVs can also form during October and November, when the climatological northeasterlies north of the equator are weaker and the climatological winds south of the equator are easterly. BVs have also been referred to as cold-surge vortices (Chen et al., 2012, 2013, 2015) and Southeast Asian sea–Maritime Continent vortices (Nugyen et al., 2016), which include the westward-propagating vortices further from the equator also known as South China Sea vortices (Howard et al., 2021).

Borneo vortices are thought to have a shallow vertical structure but can occasionally intensify into tropical storms (Koseki et al., 2014). Although they do not produce as much rain overall as tropical cyclones, they can lead to extreme events (Isnoor et al., 2019; Juneng et al., 2007; Ooi et al., 2011), and produce 50%–55% of the total precipitation in October to March over the western coast of Borneo and up to 20%–25% in the southeast of Peninsular Malaysia (Liang et al., 2021). The interactions between BVs and cold surges have been investigated by Chang et al. (2005), Koseki et al. (2014), Chen et al. (2015), Lim et al. (2017) and Liang et al. (2021). The frequency of BVs increases on cold-surge days (Liang et al., 2021). The presence of the cold surge increases shear vorticity and increases moisture convergence near Borneo, thereby enhancing the BV (Koseki et al., 2014). On days with no cold surge, anomalous vorticity is maximised further north across the South China Sea. On no-vortex days, there is increased interaction between winds and topography and convection is enhanced across Sumatra and Peninsular Malaysia, while it is reduced in the South China Sea. On vortex days the opposite occurs, and rainfall is greater near Borneo and Thailand (Chang et al., 2005). The presence of a cold surge enhances this shift in rainfall further. Chen et al. (2015) showed that the location of the formation of a cold-surge vortex is dependent on the location of the low-level trough and the type of cold-surge flow. A shallow surface trough east of the Philippines plus a more easterly cold-surge flow is required to form vortices near the Philippines, whereas a near-equator trough with northeasterly shear flow plus a meridional cold-surge flow, which can deepen the near-equator trough, leads to formation of vortices near Borneo. The type of cold-surge flow can also either hinder or facilitate vortex propagation. When northerly flow is greater than easterly flow, propagation is hindered, whereas when easterly flow is greater than northerly flow, vortices are more likely to propagate westwards into Peninsular Malaysia and Thailand.

Large-scale weather modes are also known to impact the rainfall in the Maritime Continent region (e.g., the Madden–Julian Oscillation [MJO]: Wang & Rui, 1990; Jeong et al., 2008; Peatman et al., 2014; Xavier et al., 2014; Birch et al., 2016; Muhammad et al., 2020; DaSilva & Matthews, 2021, and equatorial waves: Lubis & Jacobi, 2015; Ferrett et al., 2020; Lubis & Respati, 2021). Chang et al. (2005), Lim et al. (2017) and Liang et al. (2021) investigated the interaction between BVs and the MJO. When the MJO has its convectively active phase centred over the eastern portion of the Maritime Continent, cold-surge frequencies are reduced. This is due to the westerly wind anomalies in this phase of the MJO opposing those of the cold surge, although, the cold surge is a more dominant feature than the MJO. When the cold surge and active MJO occur simultaneously, however, the more moist and less stable conditions of the active MJO result in significantly more rainfall than when there is only a cold surge (Liang et al., 2021; Lim et al., 2017). BVs were found to have higher frequencies, stronger maximum low-level wind speeds and longer lifetimes during combined cold surge and active MJO conditions compared to any conditions (Liang et al., 2021).

Case studies of a small number of BVs suggest they can extend to 300 hPa. However, little is known about their structure more generally and how cold surges and equatorial waves affect them. The rainfall in this region is notoriously difficult to forecast. However, forecast models

are better able to predict large-scale weather regimes (Gonzalez et al., 2023) and equatorial waves (Yang et al., 2021). An understanding of how the frequency, location and rainfall of BVs is modified by these large-scale phenomena will aid forecasters in their predictions of rainfall. In this study we examine a 41-year database of BVs and use clustering methods to identify different types of vortices based on track location (Section 3.1). We show how the seasonality of large-scale flow (Section 3.2), surge conditions (Section 3.3), the MJO (Section 3.4) and equatorial wave conditions (Section 3.5) affect the frequency of these different clusters. We also examine how the associated rain of these vortices is modified by different surge conditions, the MJO and equatorial waves. We then examine the detailed structure, lifetime, and the associated rain of representative case studies in each cluster (Section 3.6).

2 | DATA AND METHODS

We use the ERA5 reanalysis dataset (Hersbach et al., 2020) to identify and track BVs, to determine cold surges and to analyse the structure of BVs. At the time of doing the tracking, ERA5 data were available from 1979 to 2022. The data used is hourly, on a 0.25° longitude–latitude grid with average grid spacing of 31 km in the tropics and on 37 different pressure levels.

2.1 | Identification and tracking of Borneo vortices

There is no single way to identify BVS. Some studies have looked for closed circulations in the 925-hPa stream function within a region surrounding Borneo (e.g., Chang et al., 2005 used 2.5° S–7.5° N, 107.5°–117.5° E), sometimes with winds exceeding a particular threshold (e.g., Chang et al., 2005; Chen et al., 2012, 2013, 2015; Howard et al., 2021). Other studies have tracked low-level relative vorticity and found those vortices that spend some time within a similar region near Borneo (e.g. Howard et al., 2021; Liang et al., 2021).

Here we use the TRACK tracking algorithm (Hodges, 1994; Hodges, 1995; Hodges, 1999) to identify and track vortices in the region using spatially filtered six-hourly 850-hPa relative vorticity (ζ) obtained by spectral truncation to T63, during October–March from 1979 to 2022. The tracking is also performed for 925-hPa ζ. This is the same tracking algorithm as used by Liang et al. (2021) and has also been used to track tropical and extratropical cyclones, tropical easterly waves, polar lows, and Tibetan Plateau vortices (for references see Liang et al., 2021). The tracked ζ at the centre of the vortex is hereafter referred to as ζ_c. To identify BVs, we look for those 850-hPa vortices that initiate within 5° S–12° N, 100.0°–125° E, spend at least a day within 2.5° S–10° N, 100.0°–117° E (hereafter referred to as our BV region, that is, an extended region compared to that used by Chang et al., 2005), and that reach a maximum ζ_c of at least $3.5\times10^{-5}\,s^{-1}$. We also require that the vortex is seen in the 925-hPa tracks for some of the lifetime to indicate a coherent structure over more than one pressure level. The 925-hPa and 850-hPa vortex centres of the same Borneo vortex may be located more than 1° apart due to the vortex tilting. Therefore, we match the 850-hPa tracks to the closest 925-hPa track that is within 2° of the 850-hPa track centre. We remove any vortices that are tropical cyclones by matching our tracked centres with tropical cyclone tracks from the International Best Track Archive for Climate Stewardship (IBTrACS; Knapp et al., 2010) that are within 3° at any time (note that the IBTrACS centre is measured at the surface whereas our centre is at 850 hPa so we do not expect an exact match). This removal process includes removing the vortex described in Koseki et al. (2014) that became tropical cyclone *Vamei* (2001). Removing vortices that match a tropical cyclone after they have been in our BV region (and, therefore, may be considered by some to be BVs) is unlikely to alter our conclusions given that such vortices only form 1.4% of the population. We use our extended region so that we can also examine vortices that propagate across the region further north than the more stationary BVs examined by Chang et al. (2005) and we put a lower limit on the maximum ζ_c so that we only look at features of a suitable intensity. To match the available dates in the weather regime and equatorial wave datasets, we use the tracking data from 1980 to 2021 (41 years). During the 7655 days (October–March) between 1980 and 2021 we identified 613 BVs.

2.2 | Identification of weather regimes

We use the two-tier weather regime dataset of Howard et al. (2021) which covers the period 1979–2021. This dataset is based on clustering of ERA5 winds and the tier1 planetary regimes (eight regimes labelled R1 to R8) describe the large-scale seasonal flow (see Figure 3 of Howard et al., 2021), whereas the tier2 regimes (not examined here) describe regional patterns within the tier1 regimes. R1 and R2 take place mostly in January and February during the austral monsoon and northeast Asian monsoon, when there are westerlies just south of the equator, with R2 representing more La Niña-like conditions and R1 representing more El Niño-like conditions; R3 is a transition season occurring mostly in April when the intertropical convergence zone (ITCZ) moves northwards; R4 and R5 mostly occur from May to September

when meridional winds in the northern hemisphere (NH) are mostly southwesterly (boreal summer monsoon) and there are easterlies just south of the equator; R6 occurs in September–October during the retreat of the Boreal monsoon; R7 occurs in October to November when the ITCZ moves southwards; R8 occurs mostly in November to December during the onset of the austral monsoon.

2.3 | Identification of cold surges

Cold-surge indices have previously been determined using low-level winds, with either just the northerly component (e.g., Chang et al., 2005) or also including the easterly component (e.g., Koseki et al., 2014; Lim et al., 2017). These winds are averaged typically over 110°–115° E but may be measured at 15° N or averaged over various latitudes from 5° to 12.5° N. The exceedance of either a fixed threshold or one based on standard deviations from climatology have been used. Hattori et al. (2011) defined a cross-equatorial surge as when the northerly wind at 5° S averaged over 105°–115° E exceeds 5 $m \cdot s^{-1}$.

Based on the definitions of Chang et al. (2005), Koseki et al. (2014), Lim et al. (2017) and Hattori et al. (2011) we define three types of cold surge (also used by Howard et al., 2021) using daily mean ERA5 925-hPa winds and categorising the cold surges further into weak, moderate, and strong as follows:

- A meridional surge occurs when the northerly wind (magnitude of v) at 15° N averaged over 110°–117.5° E is within the ranges:
  - Weak: $8 < v \leq 10\ m \cdot s^{-1}$
  - Moderate: $10 < v \leq 12\ m \cdot s^{-1}$
  - Strong: $v > 12\ m \cdot s^{-1}$
- An easterly surge occurs when the easterly wind (magnitude of u) averaged over 7.5°–15° N at 120° E is within the ranges:
  - Weak: $8 < u \leq 10\ m \cdot s^{-1}$
  - Moderate: $10 < u \leq 12\ m \cdot s^{-1}$
  - Strong: $u > 12\ m \cdot s^{-1}$
- A cross-equatorial surge occurs when the northerly wind averaged over 0°–5° S and 105°–115° E, $v > 5\ m \cdot s^{-1}$.

2.4 | Identification of the MJO index

We use the Bureau of Meteorology real-time MJO tracking dataset (http://www.bom.gov.au/climate/mjo/graphics/rmm.74toRealtime.txt) which divides the MJO into eight real-time multivariate (RMM) phases (Wheeler & Hendon, 2004). We considered any day with MJO amplitude greater than or equal to 1.0 to be an 'active' MJO day. The eastward-propagating MJO is convectively active over the Maritime Continent during phases 3, 4, and 5, whereas suppressed convective activity occurs for the other phases. Therefore, we examine phases 3–5 together and phases 1, 2, 6–8 together and compare with inactive phases.

2.5 | Identification of equatorial waves

We use the equatorial wave dataset of Yang et al. (2023) which is based on ERA5 winds and designed to cope with a background flow with vertical wind shear. This dataset has been developed using the methodology of Yang et al. (2003) which has been shown to perform well against other identification methods (Knippertz et al., 2022). Equatorially trapped waves are obtained as solutions to the adiabatic, frictionless equations of motion on an equatorial β-plane linearised about a state of rest. This dataset, which covers the period 1980–2020, was created by projecting the dynamical fields in the tropics at each pressure level onto a set of horizontal structures described by a Fourier decomposition in the x-direction and parabolic cylinder functions in the y-direction, forming a set of orthogonal horizontal modes (wave types). From this dataset, we reconstruct u and v components for the three main wave types: eastward-moving Kelvin waves (KWs), westward-moving mixed Rossby–gravity waves (WMRG) and westward-moving $n = 1$ Rossby waves (R1). The data is six-hourly on a $1° \times 1°$ grid; however, we average over 5° in the longitude to smooth the data in line with Ferrett et al. (2023). These waves are characterized by wave variables w_1 and w_2 as shown in Table 1; w_1 and w_2 are normalised by their standard deviations to give W_1 and W_2, and if the amplitude $({W_1}^2 + {W_2}^2)^{0.5}$ is greater than 1, the wave is identified as present (Ferrett et al., 2023; Yang et al., 2021). The Kelvin wave propagates eastward, and the variables are defined so that w_2 is positive one quarter of a wavelength ahead (east) of w_1 positive. Note that $-u$ is used to define w_1 (rather than u) for WMRG and R1 waves because these waves propagate westward and w_2 is defined so that it is positive one quarter of a wavelength ahead (west) of w_1 positive.

2.6 | Analysis of the vortices

We investigate the relationships of Borneo vortex frequency with the seasonality of the large-scale flow, the cold-surge index from 1980 to 2021, the MJO RMM index

TABLE 1 Characterization of equatorial waves using two wave variables, each evaluated at the latitude of its maximum in the corresponding meridional structure function for each wave type. See text for more details.

	w_1	w_1 latitude	w_2	w_2 latitude
Kelvin waves	u	0° N	$\partial u/\partial x$	0° N
WMRG waves	$-u$	10° S	v	0° N
Rossby 1 waves	$-u$	0° N	v	8° N

Abbreviation: WMRG, Westward-moving mixed Rossby–gravity (WMRG).

from 1980 to 2022, and with equatorial waves from 1980 to 2020. To determine the rainfall associated with the BVs, we use the Integrated Multi-satellitE Retrievals for the Global precipitation measurement mission (GPM) dataset (IMERG; Huffman et al., 2020). The IMERG algorithm combines data from a network of partner satellites equipped with passive microwave and infrared sensors and fuses the early precipitation estimates collected during the operation of the Tropical Rainfall Measuring Mission satellite (2000–2015) with more recent precipitation estimates collected during operation of the GPM satellite (2014–present). The IMERG product has been shown to match station data well up to the 95th percentile over Southeast Asia (DaSilva & Matthews, 2021). Data are available at 30-min intervals on a 0.1° × 0.1° horizontal grid. We calculate rain associated with a Borneo vortex, R_a, by taking the mean within a radius of 4° around the vortex centre. Since IMERG is not available before 2000, we perform our rainfall analysis on the vortices from 2000 onwards.

We categorised our BVs according to their track using k-means clustering. K-means clustering requires the same number of parameters for each member of the population. We therefore took six evenly spread sample locations from each track, which required the vortices to have a lifetime of at least 36 h, reducing our population from 613 to 585 vortices. As we will show, the different clusters tend to occur under different weather regimes and surge conditions.

To examine statistically how the track frequency (F_s) of BVs in each cluster is modified by cold surges and equatorial wave phases, we count all the time points when each Borneo vortex in that cluster is in each surge condition or wave phase (n_s) and divide by the number of six-hour time points that the condition exists over our whole 41 years (N_s), that is, our population for each surge condition or wave phase is a set of single frequency values (f_s) for each Borneo vortex in the cluster,

$$f_s = 100 \times \frac{n_s}{N_s}, \tag{1}$$

and the overall frequency in each condition (F_s) is then the sum of these individual vortex frequencies,

$$F_s = \sum 100 \times \frac{n_s}{N_s}, \tag{2}$$

where s refers to surge type or equatorial wave phase.

Likewise, we calculate a frequency for all times regardless of surge type or equatorial wave phase as the number of time points that each Borneo vortex in the cluster exists (n_{all}) divided by the total number of time points in the 41 years (N_{all})

$$F_{all} = \sum 100 \times \frac{n_{all}}{N_{all}}. \tag{3}$$

To examine vortex averaged rain rates, R_a, and relative vorticity at the centre of the vortex, ζ_c, we take all the values when each Borneo vortex is in each surge condition or wave phase as our populations, and to obtain an overall value, we take the mean of all the R_a and ζ_c values in the population. To determine whether a property is significantly higher or lower during a surge or wave phase condition compared to all times, we use a Welch's t-test to compare the populations in the surge or wave phase condition with the population for any condition. To examine initiation frequencies, we only have a one or zero value for whether each Borneo vortex in the cluster initiates in each surge or wave phase condition ($n_s = 0$ or $n_s = 1$ in Equations 1 and 2). To obtain the actual initiation frequency we simply add up the n_s values as in Equation (2), but to determine significance of differences in initiation frequencies, we use a bootstrapping technique to randomly subsample the Borneo vortex population 1000 times using 70% of the population and in each subsample we count the initiations in each surge or wave phase condition and divide by the number of six-hourly time periods that the condition exists over our whole 41 years. These subsample frequencies are then used in a Welch's t-test to look for significance of differences in initiation frequencies compared to all times. For cold surges and equatorial waves, we present initiation and track frequencies in different states as relative changes compared to all times, calculated as,

$$\Delta F_r = 100 \times \left[\frac{F_s}{F_{all}} - 1\right], \tag{4}$$

where F_{all} is the frequency for all times defined in Equation (3).

We examined the detailed structure of a subset of the BVs by choosing BVs that occurred since January 2018, lasted for at least three days and that also had rainfall exceeding 1.2 mm·h^{-1} at some point. This resulted in 23 BVs that covered all the different clusters and for which we examined the vertical structure of the ERA5 wind fields, ζ, and potential vorticity (PV). We also examined the time series of the mean ζ within a radius of 4° around the vortex centre (ζ_a) and the mean rain rate (R_a).

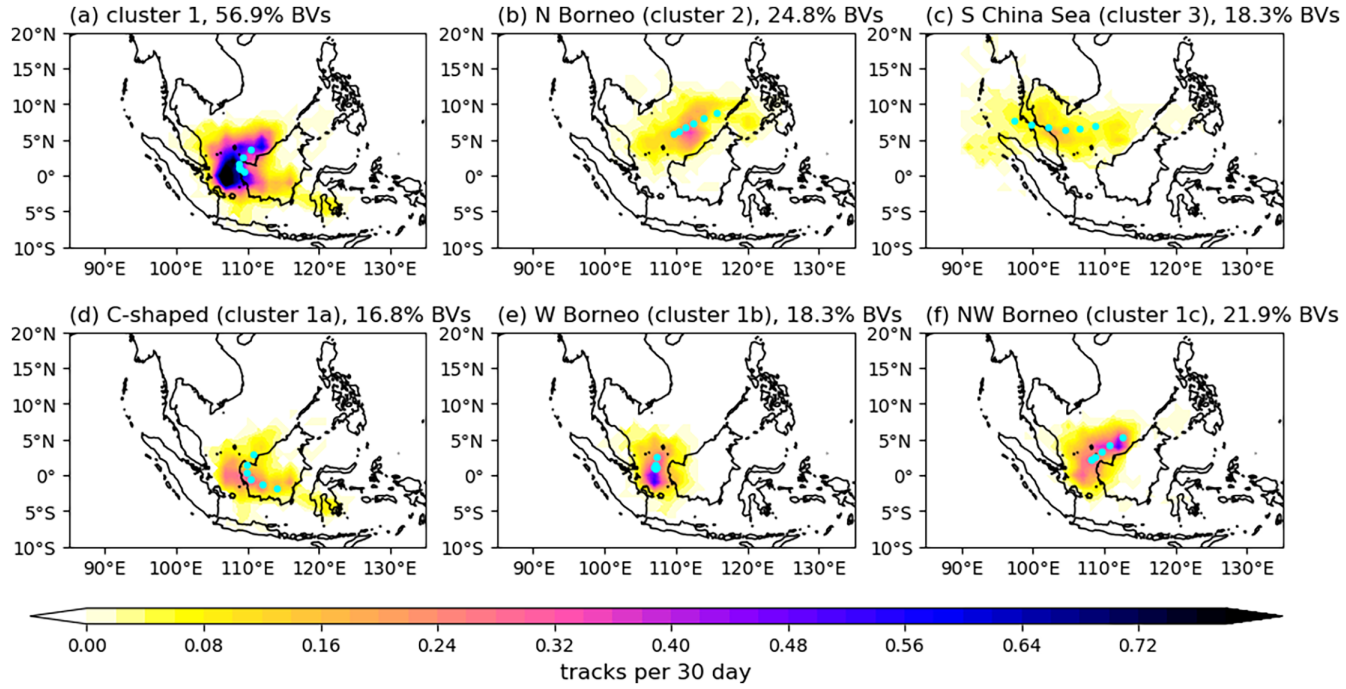

FIGURE 1 Map of Borneo vortex (BV) track frequency for the different clusters. (a)–(c) $k = 3$ clustering of all vortices; (d)–(f) $k = 3$ clustering of the vortices in cluster 1. Dots show the six track centroids of each cluster. [Colour figure can be viewed at wileyonlinelibrary.com]

We determined the vortex height and tilt by taking north–south and east–west vertical cross sections centred on the track centre at each time and finding the best estimate of the centre of rotation (i.e., winds in opposite directions either side of the centre) at each pressure level, working upwards from 850 hPa. For the east–west cross section we required positive meridional winds to the east of the centre and negative meridional winds to the west. For the north–south cross section we required positive zonal winds to the south and negative zonal winds to the north. The centre must be within ±3° of the centre in the previous pressure level. This method allows for some tilting but stops us incorrectly finding other nearby features. If at any pressure level the centre of rotation could not be found, we assumed we have reached the top of the vortex. If the vortex is not closed, we would not be able to find a centre at any height and the vortex height was set to 1000 hPa, otherwise we set the vortex height to the lowest height of the north–south and east–west cross sections. To determine the east–west and north–south tilt we used Equation (5):

$$T = \frac{c_p - c_{850}}{850 - p}, \tag{5}$$

where T is the tilt, c_{850} is the centre latitude or longitude at 850 hPa, p is the pressure level of the top of the vortex capped at 500 hPa because the vortex centres were found to shift more randomly above this level, and c_p is the centre latitude or longitude at pressure p.

3 | RESULTS

3.1 | *K*-means clustering of Borneo vortices

We used k-means clustering varying the number of clusters between 2 and 6 ($k = 2$–6) to decide how to cluster different tracks. For all values of k, one cluster was identified that initiated north of Borneo and with a track that crossed the domain to the west side of Peninsular Malaysia north of approximately 4° (i.e., South China Sea vortices that are westward-moving). For $k = 3$, the South (S) China Sea cluster emerged (Figure 1c) as did a cluster that initiated north of Borneo moving southwest towards the east side of Peninsular Malaysia (Figure 1b, North [N] Borneo cluster), but almost 57% of vortices occurred on the northwest to south side of Borneo (Figure 1a). Going beyond $k = 3$ did not effectively split this large cluster. Therefore, we stopped at $k = 3$ and subclustered this large set of vortices to obtain three more clusters as shown in Figure 1d–f. We gave names to the five different clusters shown in Figure 1 that we analyse hereafter. Clusters 1a, 1b, 1c, 2 and 3 each account for approximately 20% of Borneo vortex cases.

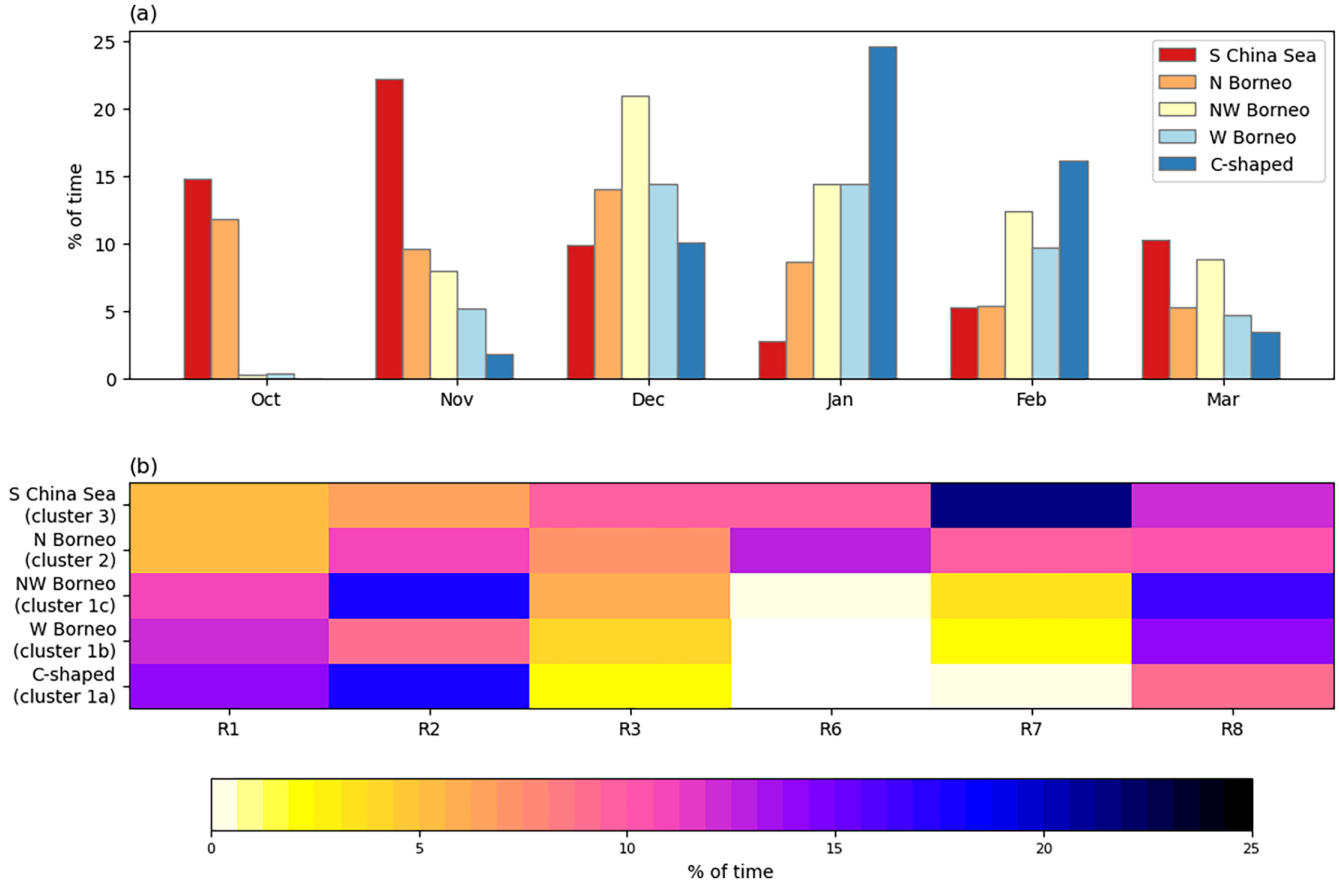

FIGURE 2 Track frequency of different Borneo vortex clusters under (a) different months (100 × vortex count/time points in month) and (b) different planetary weather regimes (100 × vortex count/time points that weather regime exists). [Colour figure can be viewed at wileyonlinelibrary.com]

The C-shaped cluster (Figure 1d) contains vortices that initiate to the north or northwest of Borneo, move to the west around Borneo and then move east again usually in the southern hemisphere (SH), spending on average more than 50% of their lifetime in the SH. Of all the clusters, we found these vortices had the lowest mean R_a and ζ_c (Figure S1). The **west** (W) Borneo cluster (Figure 1e) contains vortices that initiate in the NH on the west side of Borneo and remain on the west side of Borneo close to the equator, spending on average around 30% of their lifetime in the SH. The northwest (NW) Borneo cluster (Figure 1f) contains vortices that initiate just north of Borneo and mostly stay in the NH close to the northwest coast of Borneo, going into the SH usually for less than 10% of their lifetime. We found these vortices had the highest mean R_a of all the clusters. For most clusters we found that a larger proportion of the rain fell in the northwest quadrant (statistically significant for the S China Sea, W Borneo, and NW BVs) and a lower proportion fell in the southeast quadrant (statistically significant for all but the C-shaped BVs) (Figure S2).

3.2 | Impacts of season and planetary weather regimes on Borneo vortices

The track frequency of the different Borneo vortex clusters (F_s) shows a seasonal southward migration in the location of the vortices from October to January (Figure 2a). The S China Sea cluster peaks in November (22% of the time), the N Borneo and NW Borneo clusters peak in December (14% and 21% of the time respectively), the W Borneo cluster peaks in December and January (14% of the time) and the C-shaped cluster peaks in January (24% of the time). This is in line with southerly migration of rainfall, the low-level trough and the seasonality of the cold-surge flow (Chen et al., 2015). The track frequency in the different planetary weather regimes, R < 1–8>, for the different Borneo vortex clusters is shown in Figure 2b. We do not show R4 or R5 as these regimes correspond with the southwesterly summer monsoon flow regime when BVs do not occur. This Figure shows a similar seasonal dependence. The most northerly vortices (S China Sea cluster) are most likely to occur (23%) in R7 (October–November) when northeasterlies are weak

TABLE 2 The number of days in which a Borneo vortex (BV) exists in the given surge conditions.

		All days	No surge	Weak surge	Mod. surge	Mod. east	Mod. merid.	Mod. east + merid.	Cross eq.
Total days		7655	4064	1672	1919	883	549	95	392
Number of days in which Borneo vortex exists	All BVs	3511	1450	887	1174	519	331	79	245
	S China Sea	870	490	204	176	70	77	7	22
	N Borneo	766	377	173	216	92	62	23	39
	NW Borneo	892	305	254	333	160	105	29	39
	W Borneo	692	209	202	281	157	82	17	25
	C-shaped	728	209	177	342	105	73	12	152

in the NH and there are easterlies south of the equator and when Howard et al. (2021) found cold surges are significantly less likely to occur. S China Sea vortices are least likely to occur in R1 (January–February). The N Borneo cluster vortices are less affected by tier1 regime, although the lowest frequencies (<7%) are found in R1 and R3 and the highest frequencies (10%–13%) are found in R2, and R6. The more southerly vortices (clusters 1a–1c) are least likely to exist in R3–R7 (March–November) when Howard et al. (2021) found that cold surges are less likely to occur. C-shaped cluster vortices are most likely to occur in R2 (18%) followed by R1 (14%), that is, January–February. W Borneo cluster vortices are most likely to occur in R8 (14%) followed by R1 (12–13%), that is, November–January. The NW Borneo cluster vortices are most likely to occur in R2 (18%) and R8 (17%), regimes when Howard et al. (2021) found there was a greater frequency of meridional and easterly surges. Therefore, the impact of the planetary weather regimes on the frequency of different vortex clusters is largely through seasonality of the large-scale flow and the influence of the different surge conditions in different months. It is also worth noting that for most clusters the frequencies are higher in the R2 regime than the R1 regime, implying La Niña conditions favour BVs more so than El Niño conditions. This behaviour was also found by Chen (2002).

3.3 | Impacts of surge conditions on frequency, rainfall and vorticity of Borneo vortices

To understand the relative frequency of the cold surge and Borneo vortex phenomena we provide the numbers of days in different surge conditions and the numbers of days that the different Borneo vortex clusters exist for all days and in each of those conditions in Table 2.

Moderate cold surges exist on 1919 days, whereas BVs exist on 3511 days, showing that the Borneo vortex is a more frequent phenomenon than a moderate cold surge. The number of days with a cold surge of any strength (3591) is similar to the number of days when a Borneo vortex exists, but we found that all BVs have times of no surge during their life, showing that a cold surge is not required for a Borneo vortex to exist. We found that all NW Borneo, W Borneo and C-shaped vortices and most S China Sea and N BVs have a moderate surge at some point in their life. Table 2 shows that S China Sea vortices have more days in no-surge conditions than other clusters, whereas NW Borneo, W Borneo and C-shaped vortices have more days in moderate surge conditions than the more northerly clusters, and C-shaped vortices have considerably more days in cross-equatorial surge conditions than other clusters. We next examine these relationships in more detail by looking at the surge condition in each of the six-hourly time periods that the BVs exist rather than counting days.

Figure 3a,b shows the change in frequency in each surge condition relative to the frequency for all times for initiation and track frequencies respectively. S China Sea vortices have a low dependence on surge but are slightly more likely to initiate the weaker the surge and are unlikely to occur under cross-equatorial surges. Other types of vortices are more likely to initiate and exist with stronger surges. The N Borneo and NW BVs are most likely to initiate and exist under combined meridional plus easterly surges (297% and 92% greater frequency of initiation, and 121% and 163% greater track frequency than for all times, respectively) which would enhance the vorticity northwest of Borneo. The C-shaped vortices are most likely to initiate under meridional (147% greater frequency of initiation than for all times) or cross-equatorial surges (164% greater frequency of initiation than for all times) and are more likely to exist when there is a cross-equatorial surge (313% greater track frequency than for all times). The W

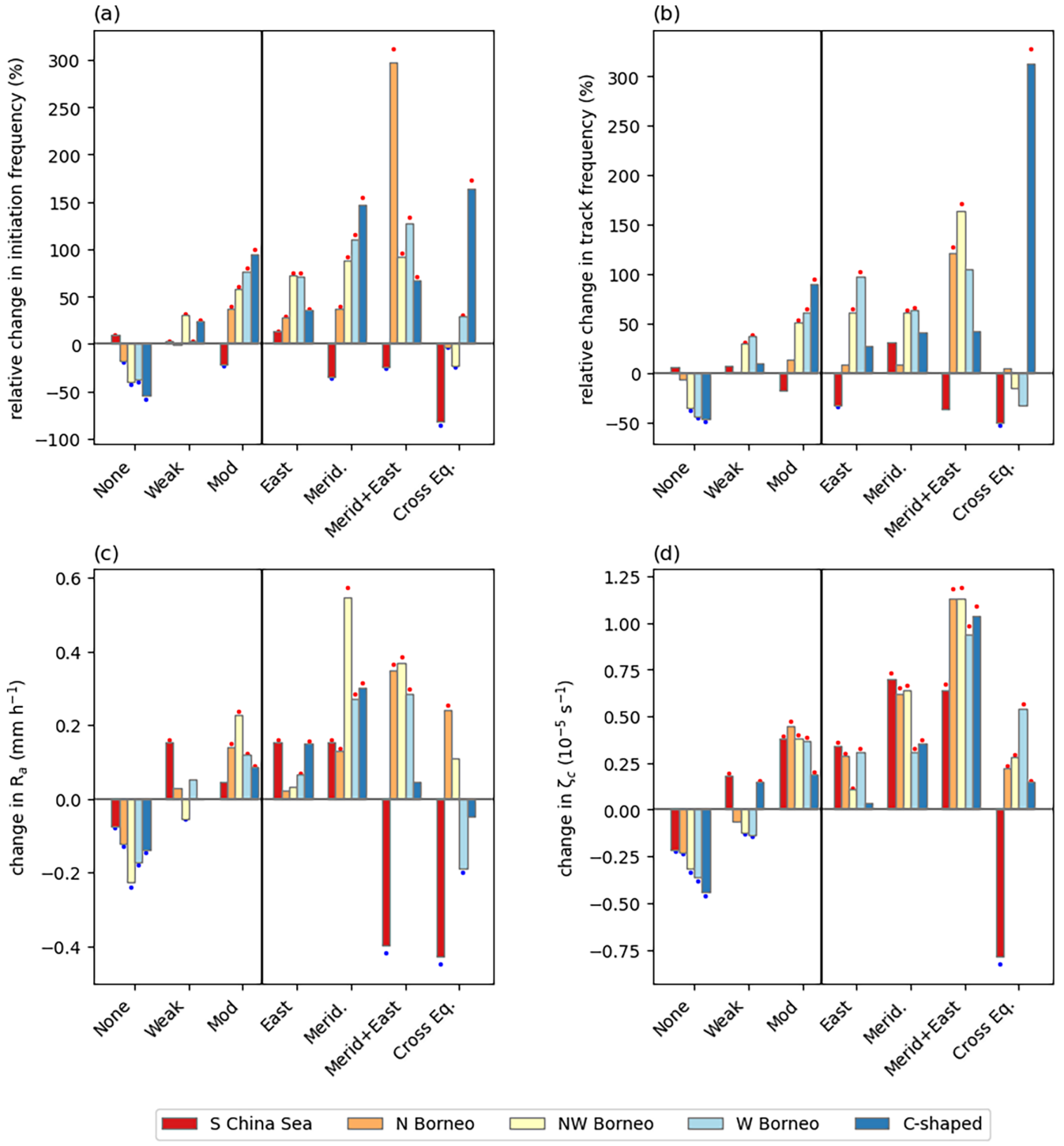

FIGURE 3 Histograms for Borneo vortex clusters' properties in different surge conditions compared to all times (Weak = weak meridional or easterly surge, Mod = moderate to strong meridional or easterly surge, or cross-equatorial surge, East = moderate to strong easterly surge only, Merid = moderate to strong meridional surge only, Merid + East = moderate to strong meridional and easterly surge only), Cross Eq. = cross-equatorial surge) for (a) relative change in initiation frequency under each surge condition, (b) relative change in the track frequency, (c) anomaly in R_a while in the surge condition and (d) anomaly in ζ_c while in the surge condition. Dots above (below) bars indicate the property is significantly higher (lower) in this surge condition than for all times. [Colour figure can be viewed at wileyonlinelibrary.com]

Borneo track frequency is strongest during easterly surges either with or without a meridional surge (over 96% greater track frequency than for all times), although initiation can be in meridional surges.

This shows that the location of BVs is strongly related to surge type. On no-surge or weak surge days, BVs are more likely to occur near Vietnam, Thailand, and the northern part of Peninsular Malaysia (i.e., S China Sea and N Borneo clusters); on cross-equatorial surge days, BVs are more likely to occur in southern Borneo (i.e., C-shaped cluster); on moderate easterly and meridional surge days, BVs are more likely to occur on the north to northwest edge of Borneo (i.e., N Borneo and NW Borneo clusters). Figure S3 shows a map of the track frequency of all BVs which also indicates the surge's influence on location.

Figure 3c shows that the rain rate, R_a, of BVs (from 2000 to 2021) is higher on moderate to strong surge days compared to no-surge days for all vortex types, although S China Sea vortices have higher R_a (0.15 mm·h^{-1} more than for all times) on weak surge days. S China Sea vortices have higher rain rates on moderate to strong meridional or easterly surge days compared to all days, whereas they have much lower R_a on moderate to strong meridional plus easterly surge days (0.40 mm·h^{-1} less than for all times) and cross-equatorial surge days (0.43 mm·h^{-1} less than for all times). The N BVs, NW BVs and C-shaped vortices have highest R_a on moderate to strong meridional surge days (0.35, 0.55 and 0.30 mm·h^{-1} more respectively than for all times) and W BVs have similarly high R_a on moderate to strong meridional surge days with and without an easterly surge (up to 0.28 mm·h^{-1} more than for all times). Using data from the Japanese Meteorological Agency reanalyses, Koseki et al. (2014) found moist static energy is anomalously transported to the equatorial South China Sea by strong cold surges. This anomalous transport would produce stronger moisture convergence, especially when meeting coastlines, resulting in heavier rain.

Figure 3d shows that the ζ_c of all BVs, except S China Sea vortices, is highest under moderate to strong meridional plus easterly surge conditions (at least 0.9×10^{-5} s^{-1} higher than for all times). S China Sea vortices have highest ζ_c on moderate to strong meridional surge days (0.70×10^{-5} s^{-1} higher than for all times) and particularly low ζ_c on cross-equatorial surge days (0.80×10^{-5} s^{-1} lower than for all times). ζ_c is lowest on no-surge and weak surge days for all vortex types except S China Sea vortices.

3.4 | Impacts of the MJO on frequency, rainfall and vorticity of Borneo vortices

Here we examine the impact of the MJO on BVs and compare those impacts with the impact of the cold surge. The track frequencies (Figure 4a) mostly increase (up to 25% relative increase) in MJO phase 3–5 and decrease in other active phases, although not all clusters behave the same. This is a considerably smaller increase than that caused by a cold surge where relative increases of 15%–90% occur. However, the combination of the MJO phase 3–5 and a cold surge enhances track frequencies further (up to 125%). This is in agreement with previous studies (Liang et al., 2021; Lim et al., 2017).

The R_a of all Borneo vortex clusters (Figure 4b) increases during MJO phase 3–5 (0.12 mm·h^{-1}) and decreases in other active phases (−0.08 mm·h^{-1}). This is comparable with the change in R_a due to a cold surge but is more consistent between the different vortex clusters. The combined MJO phase 3–5 and cold surge enhances R_a further for all clusters except the S China Sea cluster. This increase is due to the more moist and less stable conditions of the active MJO in phase 3–5.

The ζ_c of most Borneo vortex clusters (Figure 4c) increases during MJO phase 3–5 and decreases in other active phases. This is comparable with the change in ζ_c due to a cold surge. The combined MJO phase 3–5 and cold surge enhance ζ_c further for all clusters. This is consistent with the impacts of the MJO on maximum low-level winds in BVs found by Liang et al. (2021).

3.5 | Impacts of equatorial waves on frequency, rainfall and vorticity of Borneo vortices

The rotational WMRG and R1 waves, have the following phases at a given location: strong southerly wind (WMRG v_{0N}+ and R1 v_{8N}+), strong westerly wind (WMRG u_{10S}+ and R1 u_{0N}+), strong northerly wind (WMRG v_{0N}- and R1 v_{8N}-), and strong easterly wind (WMRG u_{10S}- and R1 u_{0N}−). Therefore, depending on the location of the wave, these waves may enhance or counteract the climatological northeasterlies and the cross-equatorial flow, and therefore, modify the strength of cold surges. Kelvin waves only affect the zonal wind, having the following phases: strong westerlies (KW u_{0N}+), strong zonal divergence (KW div_{0N}), strong easterlies (KW u_{0N}−) and strong zonal convergence (KW $conv_{0N}$) and therefore would only be expected to modify the easterly surge, although also have a small amount of associated vorticity. Through modification of the surge, the frequency of BVs may be modified. However, WMRG and R1 waves are rotational in character and can provide enhanced vorticity in the WMRG u_{10S}+ phase and R1 u_{0N}+ phase in the NH and R1 u_{0N}− phase in the SH.

To estimate initiation and track frequencies of BVs in each of the different equatorial wave phases, we need the

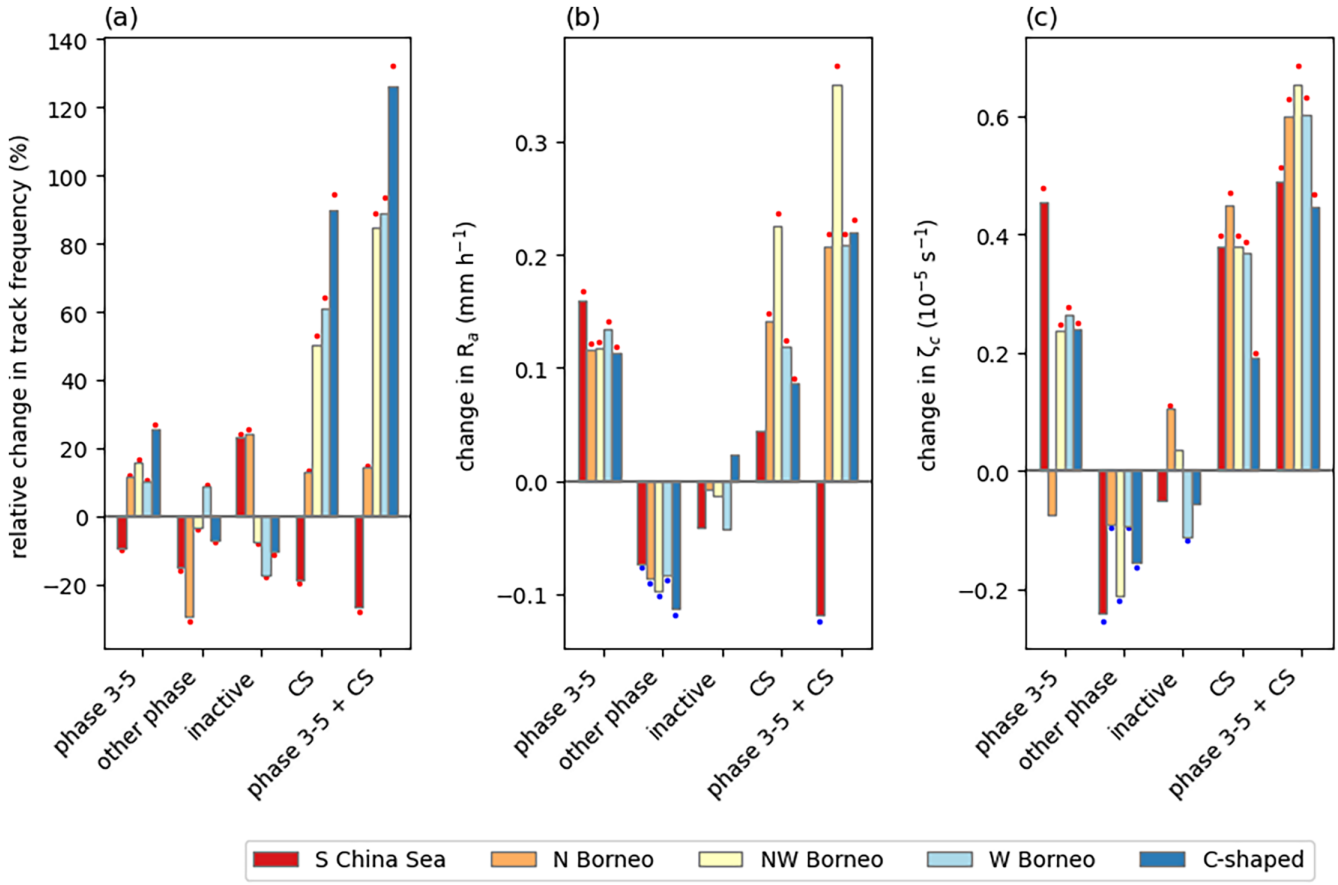

FIGURE 4 Histograms for Borneo vortex clusters' properties in different MJO phases compared to all times for (a) relative change in the track frequency, (b) anomaly in R_a while in the condition and (c) anomaly in ζ_c while in the condition. Dots above (below) bars indicate the property is significantly higher (lower) in this condition than for all times. Anomalies while in any moderate to strong cold-surge condition (CS) and while in the combined MJO phase 3–5 and moderate to strong cold-surge condition (phase 3–5 + CS) are also shown. [Colour figure can be viewed at wileyonlinelibrary.com]

time that each wave phase occurs. We determined the number of times each wave phase goes through the region by counting the times in each phase of the wave at 110° E. We chose 110° E because this is in the centre of the region in which BVs exist.

Figure 5a–c shows the relative change in vortex initiation frequency and Figure 5d–f show the relative change in track frequency of different Borneo vortex clusters under different co-located wave phases. The cartoons at the bottom of each panel are there to aid the reader in visualising the phase of the waves. Although KWs can influence the initiation of BVs (e.g., S China Sea and WBV 'BVs' N have 30% and 25% respectively greater initiation frequencies in the Kelvin convergence phase compared to all times, and C-shaped vortices have 38% greater initiation frequencies in the Kelvin $u_{0N}-$ phase than all times), KWs have little effect on their persistence, except for C-shaped vortices which have 38% greater track frequencies than for all times in the convergence phase. C-shaped vortices spend some time moving eastwards so can move with a Kelvin wave. We show this occurring in a case study in Section 3.6.1. Borneo vortex initiation and existence is strongly affected by WMRG waves: S China Sea vortices have 68% greater initiation frequencies and 81% greater track frequencies than for all times within the WMRG $u_{10S}+$ phase (positive vorticity), implying that these vortices move in phase with these waves. They are also quite likely to initiate on the leading edge ($v_{0N}-$ phase) of the $u_{10S}+$ phase and spend time on the trailing edge ($v_{0N}+$ phase) of the $u_{10S}+$ phase. For all other clusters, the WMRG southward meridional flow is important for initiation with the $v_{0N}-$ phase statistically significantly enhancing the frequency of initiation (between 27% and 60% greater initiation frequencies than for all times), and the northward $v_{0N}+$ phase statistically significantly reducing the initiation frequency (up to 47% lower initiation frequencies than for all times). C-shaped vortices have lowest initiation frequencies in the WMRG $u_{10S}+$ phase (48% lower than for all times), which may be due to these conditions making it preferable for the vortex to form slightly further north, for example, a NW Borneo

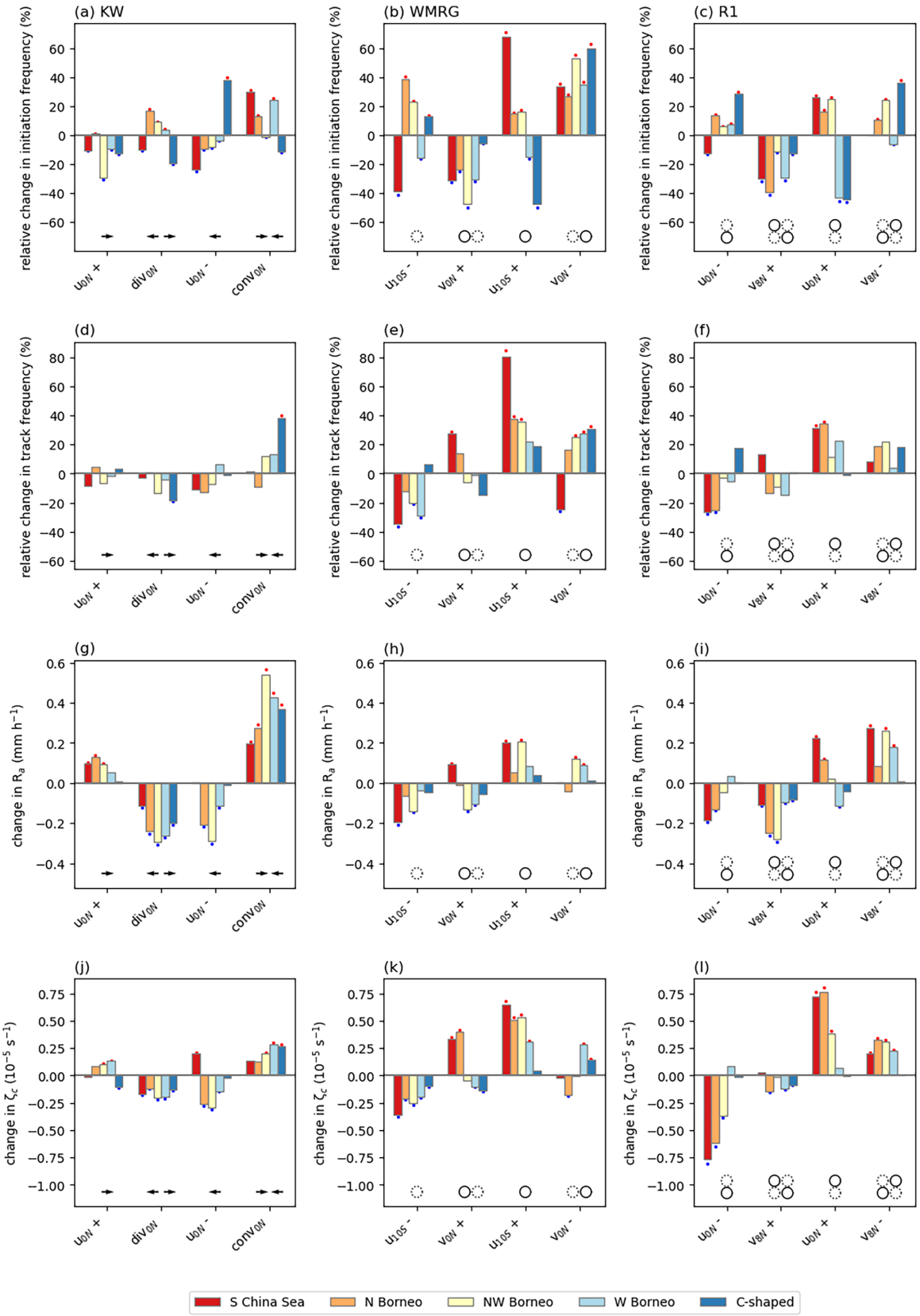

FIGURE 5 Histograms for BV clusters in different phases of equatorial waves compared to all times of (a–c) initiation frequency, (d–f) track frequency, (g–i) R_a and (j–l) ζ_c for KWs (left column), WMRG waves (middle column) and R1 waves (right column). Cartoons at the bottom of each plot are intended to help visualise the phase of the wave, with arrows indicating zonal wind for KWs, and circles indicating positive vorticity (solid lines) and negative vorticity (dotted lines). Dots above (below) bars indicate the property is significantly higher (lower) in this surge condition than for all times. [Colour figure can be viewed at wileyonlinelibrary.com]

vortex. Track frequencies are highest in the $u_{10S}+$ (positive vorticity) phase for N Borneo and NW BVs (about 35% greater than for all times) and highest in the $v_{0N}-$ phase for W Borneo and C-shaped vortices (about 30% greater than for all times).

R1 waves have a similar albeit reduced effect to WMRG waves. W BVs have 43% lower initiation frequency in the $u_{0N}+$ phase because without a strong easterly wind but with positive vorticity, a Borneo vortex would likely initiate further east and possibly north and be classified as a NW Borneo vortex. Although not statistically significant, the C-shaped cluster has a similarly high track frequency (18% higher than for all times) in the $u_{0N}-$ and $v_{8N}-$ phases. This may be because C-shaped vortices spend at least 50% of their time in the SH where there is positive vorticity in the $u_{0N}-$ phase.

Figure 5g–i shows the R_a of different Borneo vortex clusters under different co-located wave phases. For S China Sea vortices, all wave types have a similar extent of modulation of R_a, whereas for other vortex clusters KWs have the greatest impact. For KWs (Figure 5g), R_a is significantly higher in the convergence phase for all vortex clusters (between 0.20 and 0.55 $mm{\cdot}h^{-1}$ more than for all times) and significantly lower in the divergence phase for all vortex clusters (0.10 –0.30 $mm{\cdot}h^{-1}$ lower than for all times). For S China Sea vortices R_a was 0.20 $mm{\cdot}h^{-1}$ more than for all times in the WMRG $u_{10S}+$ phase, 0.22 $mm{\cdot}h^{-1}$ more than for all times in the R1 u_{0N+} phase, and 0.28 $mm{\cdot}h^{-1}$ more than for all times in the R1 $v_{8N}-$ phase. For N Borneo and NW BVs, R_a is enhanced to a lesser extent by WMRG $u_{10S}+$ and R1 $v_{8N}-$ phases.

Figure 5j–l shows the ζ_c of different Borneo vortex clusters under different co-located wave phases. ζ_c is modified the least by KWs (Figure 5j) for all cluster except C-shaped vortices, because KWs have only a small rotational component. ζ_c for C-shaped clusters is highest in the Kelvin convergence phase ($0.25\times10^{-5}\ s^{-1}$ higher than for all times) but for other clusters ζ_c is much more affected by WMRG and R1 waves. For WMRG waves (Figure 5k), ζ_c is significantly higher in the $u_{10S}+$ (positive vorticity) phase for all vortex clusters except C-shaped clusters (0.3 to $0.62\times10^{-5}\ s^{-1}$) higher than for all times. For R1 waves (Figure 5l), ζ_c of the S China Sea, N Borneo and NW Borneo clusters is significantly highest in the $u_{0N}+$ (positive vorticity) phase (0.70×10^{-5}, 0.75×10^{-5}, and $0.35\times10^{-5}\ s^{-1}$ higher than for all times respectively). W BVs have highest ζ_c in the southward $v_{8N}-$ phase (about $0.2\times10^{-5}\ s^{-1}$ higher than for all times). The ζ_c of the W Borneo and C-shaped clusters are less affected by R1 waves as they occur further south.

In summary, WMRG and R1 waves can enhance the initiation and track frequencies, R_a and ζ_c of BVs by either enhancing the environmental vorticity or the northeasterly flow. The modification of initiation and track frequency by equatorial waves is considerably less than that by cold surges because cold-surge events last typically for a few days whereas equatorial waves are more transient and are moving through the different phases. Kelvin waves have the greatest impact on R_a and all equatorial waves have an impact on R_a of a similar order of magnitude to the impact from cold surges. WMRG waves have the biggest effect on frequency, and both WMRG and R1 waves have significant impacts on ζ_c.

3.6 | Case studies of the different vortex clusters

Of the 23 identified Borneo vortex cases since 2018, we found six S China Sea (cluster 3) vortices, two of which occurred in October under no cold-surge conditions, five cases of N Borneo (cluster 2) vortices under various cold-surge conditions, five cases of NW Borneo (cluster 1c) vortices which occurred in December to February primarily under meridional and easterly cold-surge conditions, two cases of W Borneo (cluster 1b) vortices in January and March primarily under easterly cold-surge conditions, and five cases of C-shaped (cluster 1a) vortices which occurred in December to February and were influenced by either a strong meridional or cross-equatorial cold surge. All these cases occurred under a variety of MJO phases, but it has not been possible to attribute changes in rainfall or vorticity to these MJO phases on a case-by-case basis. Here we present an example of each of these clusters from the vortices mentioned above. The tracks of these cases along with the accumulated rainfall is shown in Figure 6.

3.6.1 | C-shaped vortex

The C-shaped (cluster 1a) case vortex (Figure 6a) occurred 12–22 January 2019 and was in MJO phase 3–5 from 16 January. It formed in the NH, moved around the west coast of Borneo into the SH and then from 20 January moved east across southern Borneo. It was a closed vortex for much of its life from 12:00 UTC on 14 January until 12:00 UTC on 20 January when it extended to 500–300 hPa and it was mostly vertical apart from a tilt to the west on 20 January (Figure 7a). The ζ_a increased as the vortex moved down the north coast of Borneo, peaking on 16 January and remaining high until 12:00 UTC on 18 January, then dropping rapidly on 20 January perhaps due to the vortex going over land where winds are less and the fact that there was no cold surge just on 20 January. The R_a did

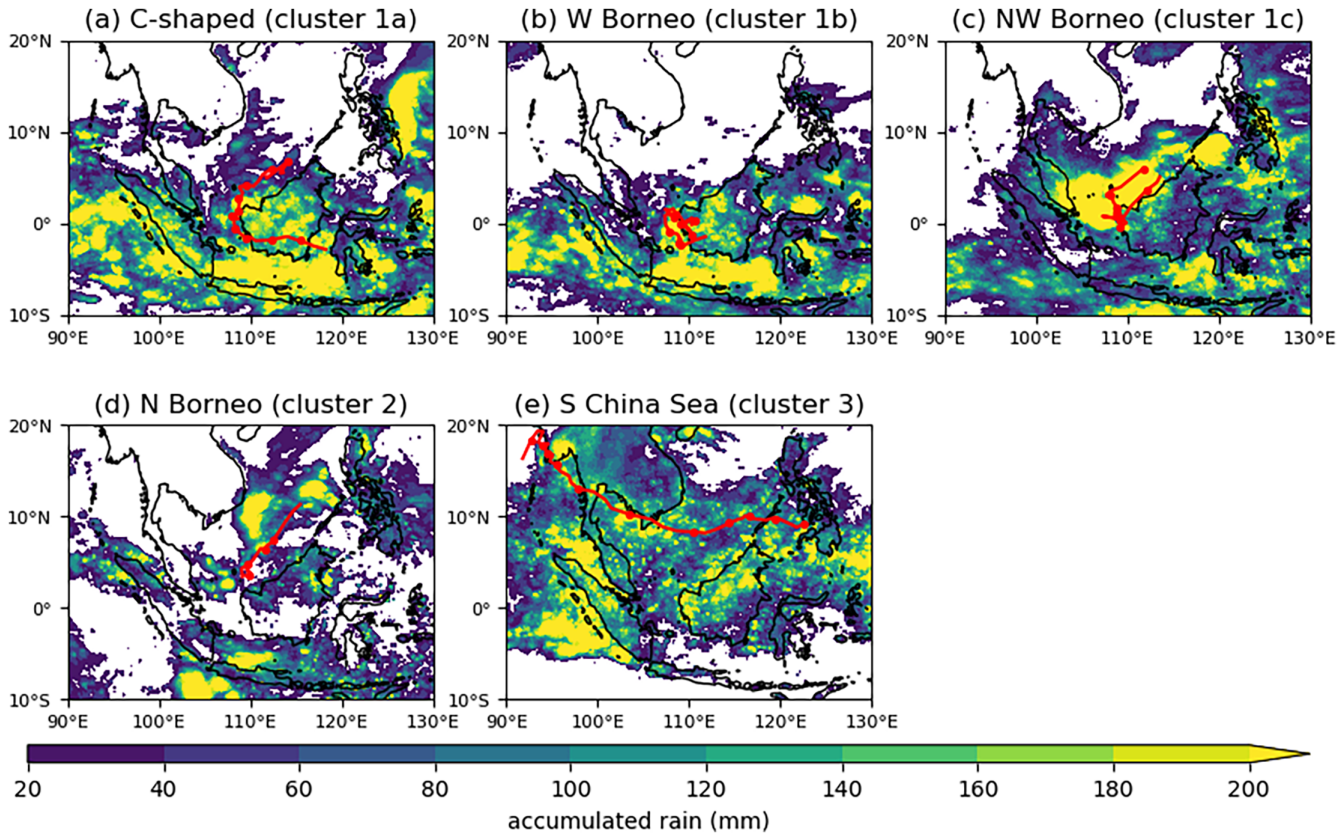

FIGURE 6 Representative cases of the five different Borneo vortex clusters showing tracks (dots connected by a line) and rainfall accumulation (shading) over the whole lifetime of the vortex. [Colour figure can be viewed at wileyonlinelibrary.com]

not follow this pattern but increased gradually with peaks on 19 January and 22 January (Figure 7c). The local minimum in R_a on 20 January coincides with the tilt to the west, the negative vorticity phase of an R1 wave (Figure 7e), and no cold surge. Despite the strong vorticity on 16–17 January, the divergent phase of a Kelvin wave became coincident with the vortex and most of the rainfall was too far from the vortex centre to be associated with the vortex (Figure 7b).

On 19 January the vortex sat in the narrowest part of the Karimata Strait (Figure 7d) where strong convergence (not shown) was produced. From 21 January the vortex was under the influence of the v_{8N}- phase of a R1 wave which enhanced the northeasterlies in the South China Sea and the convergence phase of a Kelvin wave (Figure 7e) which caused the increase in rainfall to the south of the vortex along the southern coast of Borneo and then in southern Sulawesi where it resulted in major flooding (Figure 7f). This major flooding event and its relationship to equatorial waves is examined in Latos et al. (2021). While under the influence of the Kelvin wave, the vortex moved eastwards at the same speed as the Kelvin wave.

3.6.2 | W Borneo vortex

The W Borneo (cluster 1b) case vortex (Figure 6b) occurred from 2 to 10 January 2020 staying very close to the equator. From 5 January there was an MJO phase 4. The vortex was only a closed vortex from 12:00 UTC on 4 January until 12:00 UTC on 7 January and again briefly on 9 January when it extended to 700–300 hPa and it was mostly vertical (Figure 8a). It switched from being in the SH to being in the NH and back again to the SH. The ζ_a increased rapidly peaking at 12:00 UTC on 4 January and then decreased, with R_a mostly following the same pattern apart from a very large spike of rain on the last day (Figure 8c). Before 6 January, the waves passing by the vortex were weak and not very coherent and had little effect on the rainfall. The convergence phase of a weak Kelvin wave was collocated with the vortex on 4 to 5 January, the divergence phase of the now stronger Kelvin wave was collocated with the vortex on 8 January reducing R_a, and the large peak in R_a on 10 January was due to a strong convergence phase of a Kelvin wave which coincided with the vortex. At this time, the vortex was advected eastward by the strengthened westerly flow associated with the Kelvin wave (Figure 8e).

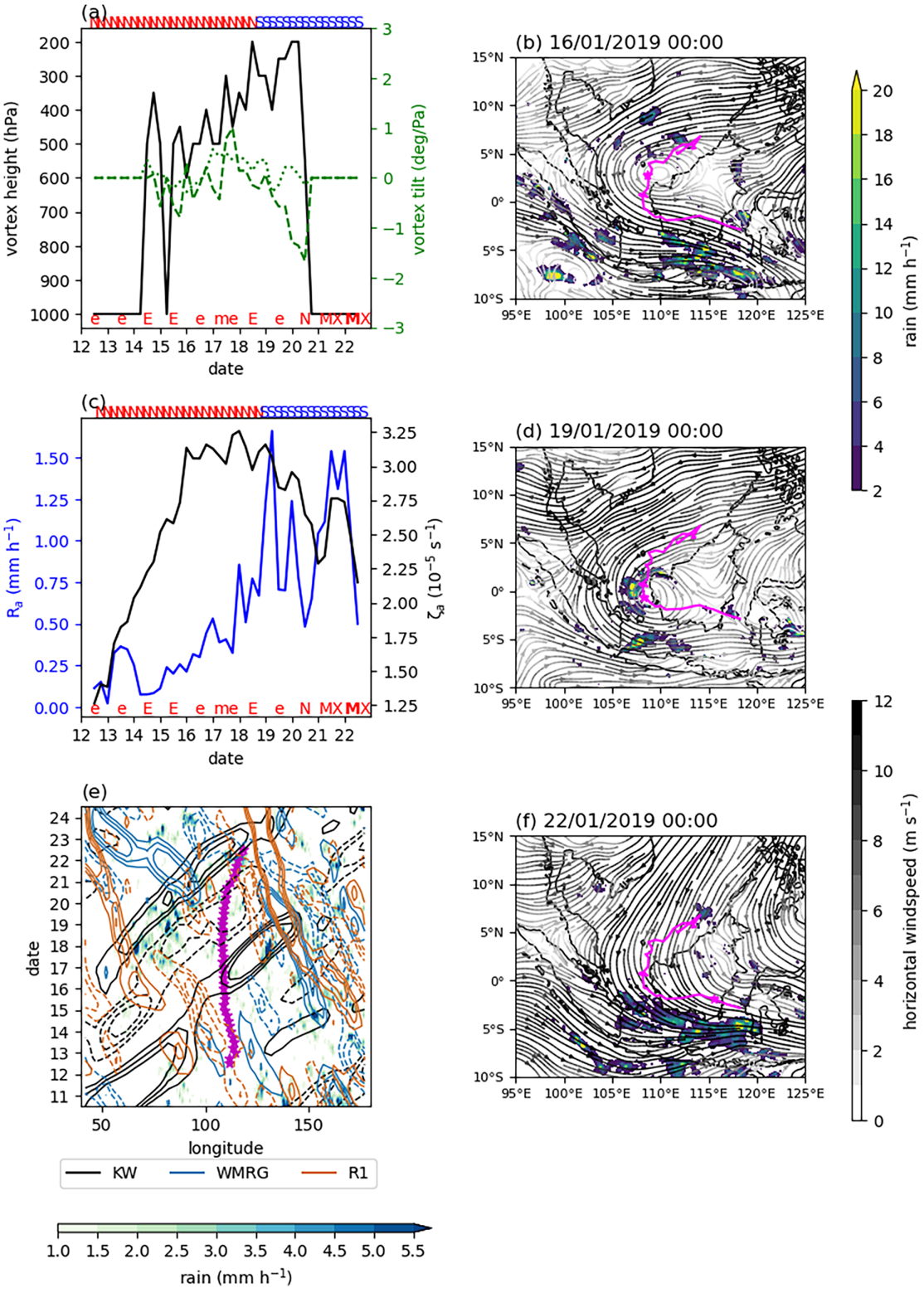

FIGURE 7 C-shaped (cluster 1a) case. (a) Time series of vortex height (solid line) and tilt (dotted line = northwards tilt, dashed line = eastwards tilt), (c) time series of R_a (blue line in online version) and ζ_a (black line in online version), (e) Hovmöller of mean rainfall average over +/− 4° centred on the vortex centre latitude, equatorial waves (solid lines show $W_2 \geq 1$, dashed lines show $W_2 \leq -1$, except for KWs which show W_1) as solid line, contours at 1, 1.5 and 2) for each wave mode, and vortex centre longitude (shown by stars (magenta online)), and (b), (d), and (f) rain and 850 hPa streamlines at three times during the vortex lifetime and vortex track and centre shown by stars and connecting line (magenta online). In panels (a) and (c) the letters at the bottom indicate the cold surge on each day (lower case means weak, upper case means moderate and bold upper case means strong; E = easterly, M = meridional, X = cross-equatorial) and the letters S and N at the top indicate in which hemisphere the vortex centre sits. [Colour figure can be viewed at wileyonlinelibrary.com]

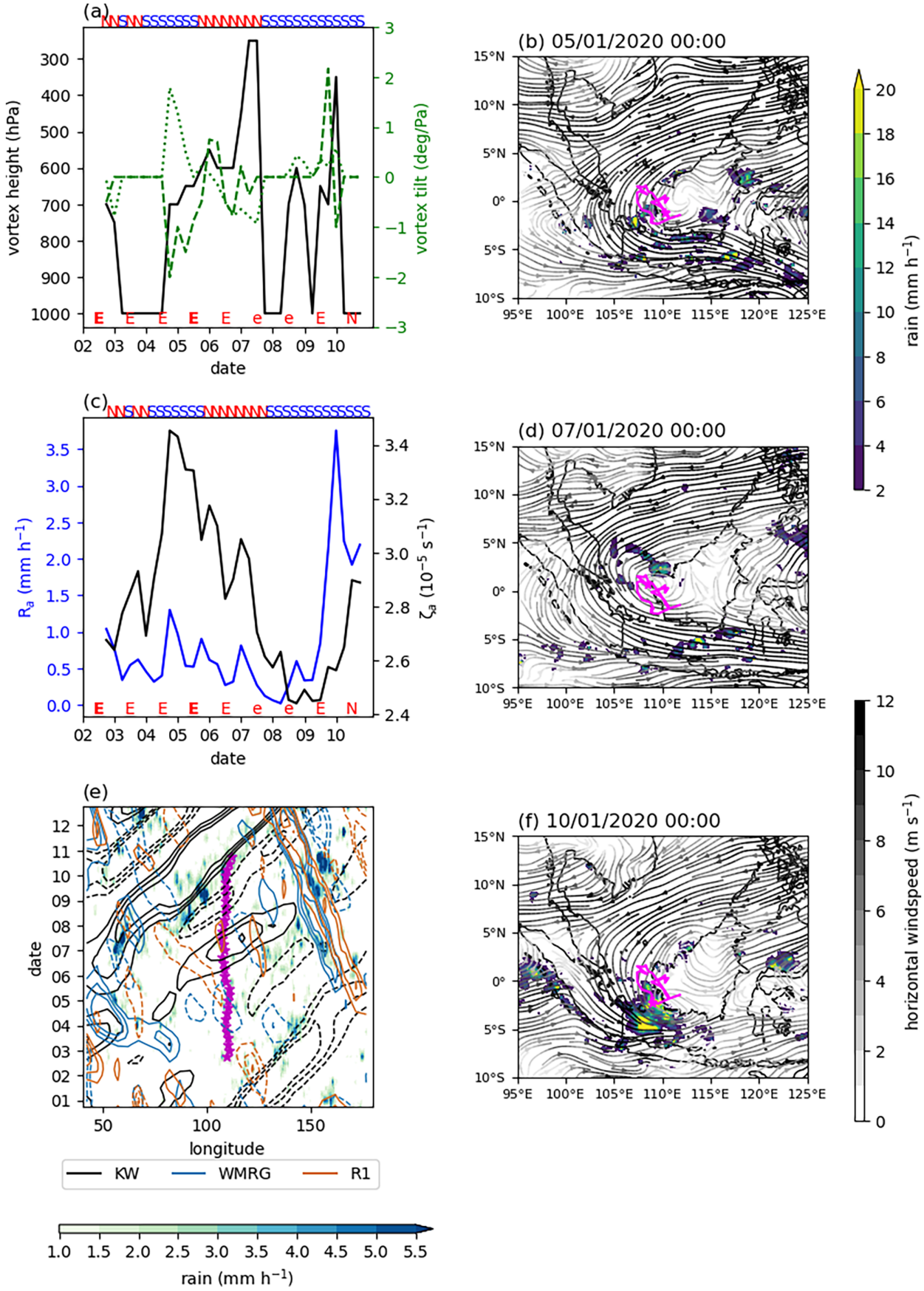

FIGURE 8 W Borneo (cluster 1b) case: as for Figure 7. [Colour figure can be viewed at wileyonlinelibrary.com]

Examples of the weaker rainfall are shown in Figure 8b,d whereas the intense rainfall caused by the Kelvin wave on 9 and 10 January is shown in Figure 8f.

3.6.3 | NW Borneo vortex

The NW Borneo (cluster 1c) case vortex (Figure 6c) was our strongest vortex in terms of ζ_a and R_a (above the 95th percentile in both) and occurred 9–16 January 2018, mostly in the NH, although briefly entering the SH on 13 January. The MJO phase changed from 2 to 3 on 13 January. It was a closed vortex for most of its life extending to 650–400 hPa and mostly vertical apart from a tilt to the west during 12 January (Figure 9a). The ζ_a increased rapidly until 12:00 UTC on 11 January, remained high until 12:00 UTC on 14 January, and then decreased, with R_a mostly following the same pattern apart from a distinct decrease during 12 January coinciding with the time during which the vortex tilted west which shifted the rain to the west (Figure 9b–d). The vortex sat within the southward flow phase of a R1 and WMRG wave (Figure 9e) for most of its life which may have been responsible for the high ζ_a and the moderate to strong meridional cold surge. This southward flow phase emerges just before the Borneo vortex initiates as a result of eastward group velocity of the packet to the west. The KWs at this time were not coherent and the strong projected Kelvin u seen near the Borneo vortex on 11 and 12 January was caused by the vortex itself moving close to the equator. The projected Kelvin u was reduced as the vortex crossed the equator on 13 January and increased again as the vortex moved back to the NH on 14 January, when the rainfall increased (Figure 9e) and high rainfall occurred mostly to the west of the vortex centre (Figure 9f). From 14 January the Kelvin projected u begins to propagate, implying the Borneo vortex has triggered the Kelvin wave.

3.6.4 | N Borneo vortex

The N Borneo (cluster 2) case vortex (Figure 6d) occurred 4–8 December 2020 under meridional and cross-equatorial surge conditions (MJO phase 4 until 5 December). It was a closed vortex for most of its life extending to 600–400 hPa and mostly vertical (Figure 10a). The ζ_a was high from the start, peaked on 6 December, and then decreased rapidly, with a smaller secondary peak on 8 December, and R_a mostly followed the same pattern (Figure 10c). The vortex formed within the positive vorticity phase of a R1 and WMRG wave which resulted in high early ζ_a and R_a (Figure 10b,d,e). As the vortex moved south, the R1 wave remained but the WMRG wave became indistinct. A strong southward WMRG flow appeared late on 5 December and the negative u phase of the Kelvin wave was distorted from around this time until 8 December which may be due to the impact of the Borneo vortex itself. The influence of this R1 wave likely became less due to the vortex moving further south. Also, initially there was a strong meridional surge, but this weakened on 6 December and by 7 December ζ_a and R_a were at a minimum (Figure 10e,f). It is not clear what caused the secondary peak in ζ_a and R_a on 8 December. KWs are less coherent during the time of this vortex and are unlikely to influence the vortex behaviour.

3.6.5 | S China Sea Borneo vortex

The S China Sea (cluster 3) case vortex (Figure 6e) occurred 15–25 October 2018 and preceded another S China Sea vortex that was examined by Hardy et al. (2023). It occurred under no-surge conditions with the MJO in phase 3 until 17 October. It was a closed vortex for most of its life extending to 500–300 hPa and mostly vertical (Figure 11a). The ζ_a increased, peaking on 19 October, and then decreased, with R_a mostly following the same pattern (Figure 11c). R_a was relatively high on 15 October (see also Figure 11b) due to the vortex coinciding with the convergence phase of a W (Figure 11e). The vortex coincided with the western edge of the $v_{0N}+$ phase of a WMRG from mid-day on 17–21 October and the western edge of the $v_{8N}+$ phase of a R1 wave from 18 to 22 October. The vortex was embedded in these waves (slightly to the west of the peak wave v), travelling at a faster speed during this time. The wave feature can be identified from the streamlines in Figure 11d and the R1 and WMRG waves produced convergence to the northwest where the rainfall was greatest. Thus, these waves enhanced both the ζ_a and R_a. Although there was a distinct Kelvin wave propagating at the time of the vortex initiation, the KW signature was not truly coherent again until 21 October. However, on 20 October the vortex sat within a Kelvin divergence phase (negative Kelvin u to the west and positive Kelvin u to the east) which may have been responsible for the minimum in R_a at this time. By 21 October this divergence phase had disappeared, and R_a increased again. By 22 October the R1 wave had dissipated, the vortex slowed down, and R_a reduced (Figure 11f). The WMRG wave seen between 18 and 22 October is part of a coherent wave packet with eastward group velocity. This wave packet is connected to the next S China Sea vortex examined by Hardy et al. (2023) which can be seen to the northeast of Borneo in Figure 11f and which initiated on 21 October at 117° E, 10° N within the $v_{0N}-$ phase of the WMRG wave.

In all these presented cases we found that the PV in the core of all the vortices was anomalously high in the lower troposphere compared to its surroundings. Hardy

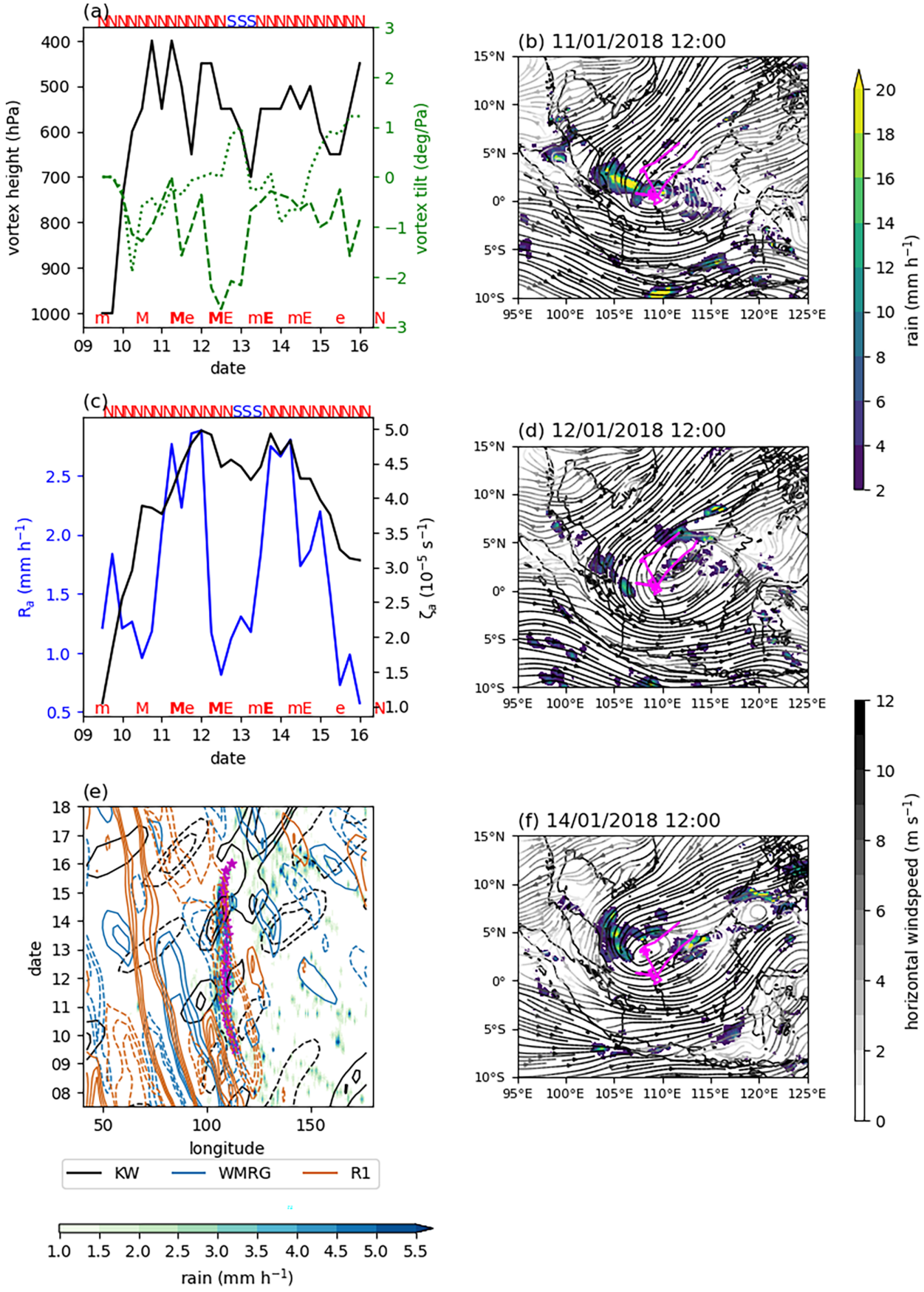

FIGURE 9 NW Borneo (cluster 1c) case: as for Figure 7. [Colour figure can be viewed at wileyonlinelibrary.com]

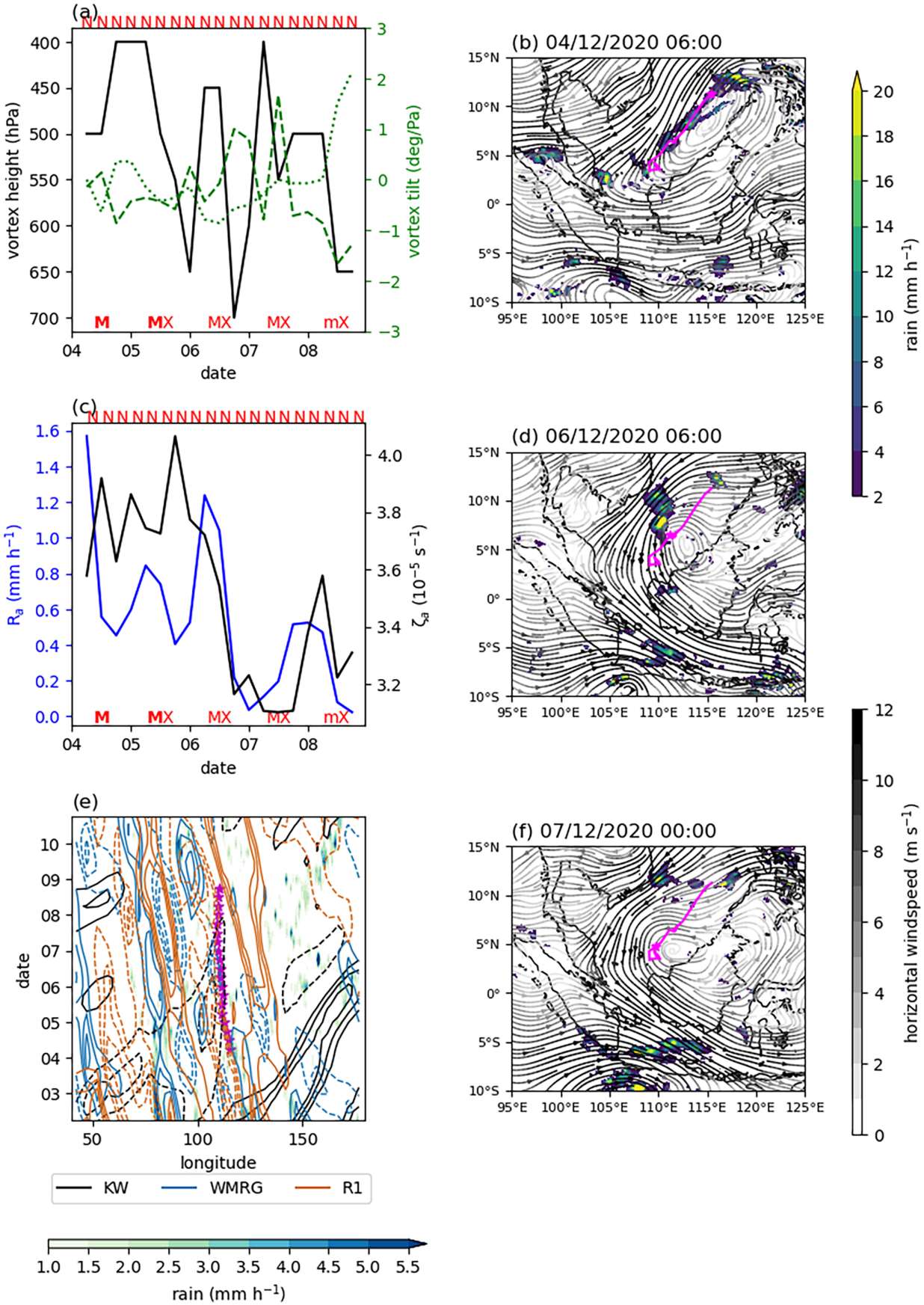

FIGURE 10 N Borneo (cluster 2) case: as for Figure 7. [Colour figure can be viewed at wileyonlinelibrary.com]

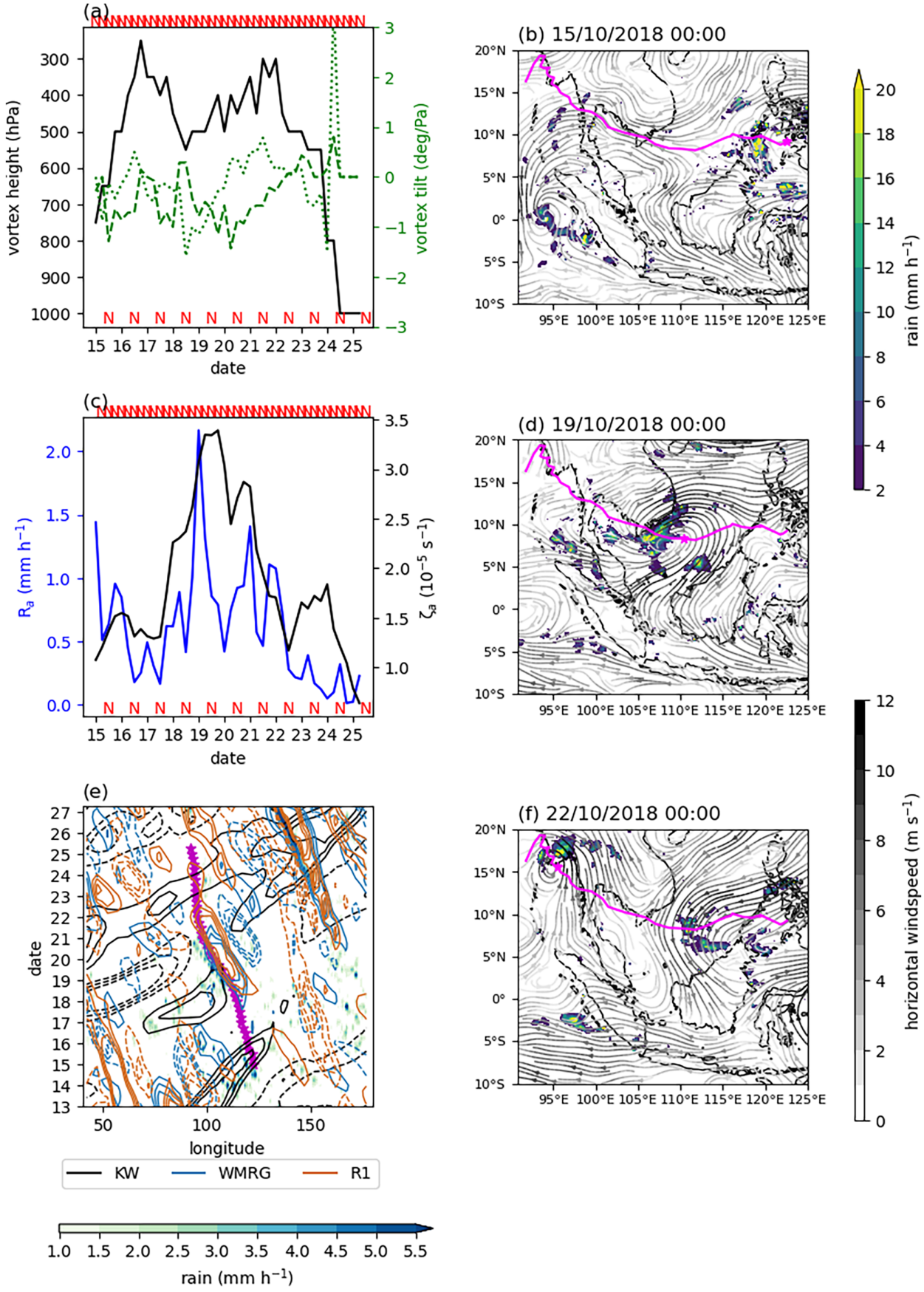

FIGURE 11 S China Sea (cluster 3) case: as in Figure 7. [Colour figure can be viewed at wileyonlinelibrary.com]

et al. (2023) provide evidence that latent heating is important to the vertical motion and low-level convergence into the vortex in their S China Sea vortex case and that vertical motion is in quadrature with the PV which contributes to the zonal propagation of the disturbance. Where the vortex crossed to the SH (W Borneo and C-shaped cases), the positive PV moved with the vortex allowing it to continue rotating anti-clockwise in an environment of weak, but negative PV south of the equator. In the W Borneo and C-shaped cases, this anti-clockwise flow appears to be important for heavy rainfall on the southwest and southern coasts of Borneo.

4 | SUMMARY AND CONCLUSIONS

We used the TRACK tracking algorithm to identify and track BVs in the Maritime Continent in October–March from 1979 to 2021 using ERA5 850 hPa relative vorticity. We used *k*-means clustering to separate the vortices into five different clusters based on track location. We explored the relationships between the frequency of the different Borneo vortex clusters and (a) seasonality/weather regimes, (b) cold surge, (c) the MJO and (d) equatorial waves and examined how rain rates and relative vorticity of the vortices were affected by cold surges, the MJO and equatorial waves. We found that planetary weather regimes affect the frequency of the Borneo vortex clusters, that is, vortex location, predominantly through the seasonality of the large-scale flow and the seasonal influence of the cold surge. We showed that the cold surge and the Borneo vortex are distinct phenomena, and all BVs experience no-surge conditions, with the vast majority also experiencing moderate cold-surge conditions. We demonstrated that the presence of a moderate to strong meridional or meridional plus easterly cold surge enhances the frequency of all vortices except the most northerly cluster. The term Borneo vortex covers different phenomena with distinct characteristics and evolution, and the clustering teases apart different types which we show have a strong seasonal dependence associated with the southward propagation of the northeasterly monsoon flow. The five clusters and their characteristics are:

1. S China Sea vortices: these are westward-propagating vortices that stay in the NH away from the equator. They occur mostly in October, November, and to a lesser extent in December and March, when the northeasterly flow is least strong. They are more frequent on no-surge days and are unlikely to occur with a cross-equatorial surge. They often initiate within the positive vorticity phase of WMRG or R1 waves. This is in line with the results of Feng et al. (2023) who found that westward-moving equatorial waves could be precursors to 60%–70% of tropical cyclogenesis events. They are typically embedded within the positive vorticity phase of westward-propagating waves, especially WMRG waves, and their rainfall and vorticity are enhanced in this phase. Their rainfall is also enhanced in the Kelvin convergence phase and the R1 NH southward flow phase. Hardy et al. (2023) have illustrated how these vortices are approximately in balance and that diabatic heating in the shear environment on the southern flank of northeasterly flow is important for their initiation and growth.
2. N BVs: these vortices form north of Borneo and move southwest parallel with the coast of Borneo. They occur mostly from October to January and are most likely to initiate and exist under combined meridional plus easterly surges. They are most likely to initiate in the southward flow phase and to exist throughout their life in the positive vorticity phase of westward-propagating equatorial waves. Their rainfall is enhanced most by the Kelvin convergence phase, but the R1 NH northward flow phase considerably reduces rainfall. Their vorticity is enhanced by both WMRG and R1 positive vorticity phases.
3. NW BVs: these vortices have similar behaviour to the N BVs but remain much closer to the coast of Borneo and occur later in the year from November to March. They also do not propagate as fast as N BVs.
4. W BVs: these vortices are quite stationary on the west side of Borneo. They occur mostly in December, January, and February, and are most likely to exist on easterly surge days either with or without a meridional surge, although they are often initiated in meridional cold surges. They are also associated with the southward flow phase of WMRG waves. Their rainfall is enhanced mostly by the Kelvin convergence phase but also the R1 NH southward flow phase. Their vorticity is enhanced by the Kelvin convergence phase, the WMRG positive vorticity phase and the R1 NH southward flow phase.
5. C-shaped vortices: these vortices initiate in the NH, move southwestwards around the western edge of Borneo into the SH and then move eastwards across southern Borneo. They mostly occur in December, January, and February, and are most likely to exist on cross-equatorial cold-surge days, although are often initiated in meridional cold surges. They are also associated with the southward flow phase of WMRG waves and the convergence phase of KW as they can move eastwards with KW when in the SH. Their rainfall and vorticity are enhanced by the Kelvin convergence phase. WMRG and R1 waves have much less effect on their rainfall and vorticity. These vortices spend more

time in the SH where the vorticity of the R1 wave is of opposite sign to that in the NH and there is very little modulation of rain rate and vorticity of these vortices by R1 waves.

Both W Borneo and C-shaped vortices retain positive PV and relative vorticity, associated with anti-clockwise rotation as they cross the equator, but they cannot be described by the same balance dynamics as S China Sea vortices since this relies on non-zero Coriolis acceleration and thermal wind balance.

We found the mean rain rates of all vortices were highest on moderate to strong cold-surge days, particularly on meridional only cold-surge days for the N Borneo cluster and on meridional plus easterly cold-surge days for NW Borneo clusters. The mean vorticity was highest under moderate to strong meridional and easterly surge conditions for all vortex clusters illustrating the importance of this type of surge for weather in the region.

The MJO has considerably less impact on the frequency of BVs than the cold surge. Statistically on the whole population of BVs, the MJO can modulate the rainfall by a similar extent to the cold surge; however, it was not possible to attribute different phases of the MJO with changes in rainfall in our representative cases. Our analysis of the impacts of the MJO are consistent with those of Lim et al. (2017) and Liang et al. (2021). The different wind anomalies for each MJO phase, shown in Lim et al. (2017) Figure 5, suggests it is likely that different clusters would be favoured in different phases of the MJO, although it is phases 3–5 that provide less stable and more moist conditions. Therefore, to gain a full understanding of the impact of the MJO on the different clusters an analysis of each MJO phase separately would be required, which was beyond the scope of this study.

The modification of the northerly and easterly flow by WMRG and R1 waves can affect where the BVs initiate and where they are likely to propagate. This modification of location along with the impact of the surge on location is in line with the results of Diong et al. (2023) who found the rainfall is enhanced on the north side of Borneo by the NH positive vorticity phase of R1 waves, and is enhanced over the southern part of Borneo (i.e., from our C-shaped vortices) by the NH negative vorticity phase of R1 waves, and that the rainfall is enhanced and shifts further south during cold surges combined with R1 waves. All clusters are favoured within or on the leading edge of the positive vorticity phase of WMRG waves. Rain rates and vorticity are also often higher in these phases of WMRG waves, especially for the more northerly vortices. KW have limited impact on the vorticity but result in higher rain rates for all clusters in the convergent and easterly phases. KW have a greater impact than R1 and WMRG waves on the rain rates, whereas R1 and WMRG waves have a greater impact on vorticity.

Our evidence suggests that the dynamics, and association with larger-scale equatorial waves, partitions BVs into two distinct classes: (i) the S China Sea, N and NW Borneo clusters are all linked with westward equatorial waves and (ii) the C-shaped and W Borneo clusters which spend most of their time on or near the equator and are more affected by KW. The cold-surge type is a key distinguishing factor between the Borneo vortex clusters within each of these two classes. The first class matches the propagating vortices of Chen et al. (2015), whereas the second class matches the quasi-stationary vortices of Chen et al. (2015) and Chang et al. (2005). Our NW BVs do not propagate as quickly as the N Borneo and S China Sea vortices and may fit in either propagating or quasi-stationary classes. Our C-shaped vortices were not discussed by Chen et al. (2015) or Chang et al. (2005) who identified BVs using closed streamlines and therefore would not have seen the latter part of the lifetime of the C-shaped vortices when they move eastwards across southern Borneo and are not closed.

We investigated the structure of 23 recent BVs covering all five clusters and under different surge conditions, and here we presented a representative case for each cluster. Vortices typically extend upward to 500–400 hPa. Those nearer the equator can reach to 300 hPa but may not always be closed vortices. Under vertical wind shear they may tilt (usually to the west). They have anomalously positive PV in their core and can cross the equator maintaining positive PV and continuing to rotate anti-clockwise. For S China Sea cluster cases, rainfall and vorticity are well correlated, with maxima occurring coincident with the NH positive vorticity phase of a R1 wave in which the vortex is embedded and moves with the wave. The wave provides greater vorticity and greater convergence to the northwest bringing heavy rain to the coast of Vietnam and Thailand. KW can dramatically increase the amount of rain when the convergence phase of the Kelvin wave is coincident with the BV, and the largest peaks in rainfall for all our cases other than the S China Sea vortices were due to a KW. However, we found that in one of our cases with a strong BV near the equator, the vortex itself can project onto the Kelvin zonal winds. It is also possible that this case was responsible for the triggering of a KW at the end of its life through the enhanced zonal flow in the region. We found the W Borneo and C-shaped cases ended as a KW propagates eastwards through the region. Although some BVs occur within a particular phase of an equatorial wave and may move in step with the phase velocity, there are also cases where BVs occur without a wave, or waves propagate through the region without a BV. In addition, the waves are periodic with multiple centres of action observed, while

we do not find more than one BV at a time associated with a wave.

Forecasting rainfall in this region is difficult whereas models are much better at predicting large-scale weather regimes and equatorial waves. Therefore, this better understanding of the relationships of BVs with cold surge, MJO and equatorial wave conditions will aid forecasters in the area to predict rainfall associated with these synoptic systems.

ACKNOWLEDGEMENTS

We thank Kevin Hodges (University of Reading) for obtaining and pre-processing the ERA-5 relative vorticity and running the tracking algorithm (TRACK) on the data. We also thank one anonymous reviewer and Goerge Kiladis for their helpful comments on our manuscript. The equatorial wave dataset was produced as part of the Newton Fund project under the auspices of the WCSSP Southeast Asia project by Dr. Gui-Ying Yang of the National Centre for Atmospheric Science, University of Reading. The ERA5 data were obtained from the Copernicus Climate Change Service, Climate Data Store, (2023): ERA5 hourly data on pressure levels from 1940 to present. Copernicus Climate Change Service (C3S) Climate Data Store (CDS), DOI: 10.24381/cds.bd0915c6 (accessed on 03-April-2023). We also acknowledge K. R. Knapp, H. J. Diamond, J. P. Kossin, M. C. Kruk, C. J. Schreck, 2018: International Best Track Archive for Climate Stewardship (IBTrACS) Project, Version 4. NOAA National Centres for Environmental Information. doi: 10.25921/82ty-9e16 (accessed 03-April-2023) for the use of the TC database.

FUNDING INFORMATION

This work was carried out as part of the FORecasting for South-East Asia (FORSEA) project, funded by the Weather and Climate Science for Service Partnership (WCSSP) Southeast Asia, as part of the Newton Fund.

CONFLICTS OF INTEREST STATEMENT

The authors have no conflicts of interest to declare.

DATA AVAILABILITY STATEMENT

The Borneo vortex database is available on request from the corresponding author.

ORCID

Julia Crook https://orcid.org/0000-0003-1724-1479
Diong Jeong Yik https://orcid.org/0000-0003-1128-7425
Gui-Ying Yang https://orcid.org/0000-0001-7450-3477

REFERENCES

Birch, C.E., Webster, S., Peatman, S.C., Parker, D.J., Matthews, A.J., Li, Y. et al. (2016) Scale interactions between the MJO and the western maritime continent. *Journal of Climate*, 29, 2471–2492. Available from: https://doi.org/10.1175/JCLI-D-15-0557.1

Chang, C.-P., Erickson, J.E. & Lau, K.M. (1979) Northeasterly cold surges and near-equatorial disturbances over the winter MONEX area during December 1974. Part I: synoptic aspects. *Monthly Weather Review*, 107(7), 812–829.

Chang, C.-P., Harr, P.A. & Chen, H.-J. (2005) Synoptic disturbances over the equatorial South China Sea and western maritime continent during boreal winter. *Monthly Weather Review*, 133, 489–503. Available from: https://doi.org/10.1175/MWR-2868.1

Chang, C.-P. & Lau, K.M. (1980) Northeasterly cold surges and near-equatorial disturbances over the winter MONEX area during December 1974. Part II: planetary-scale aspects. *Monthly Weather Review*, 108(3), 298–312.

Chen, T.C. (2002). A North Pacific short-wave train during the extreme phases of ENSO. *Journal of Climate*, 15, 2359–2376. Available from: https://doi.org/10.1175/1520-0442(2002)015%3C2359:ANPSWT%3E2.0.CO;2

Chen, T.-C., Tsay, J.-D., Matsumoto, J. & Alpert, J. (2015) Development and formation mechanism of the southeast Asian winter heavy rainfall events around the South China Sea. Part I: formation and propagation of cold surge vortex. *Journal of Climate*, 28, 1417–1443. Available from: https://doi.org/10.1175/JCLI-D-14-00170.1

Chen, T.-C., Tsay, J.-D., Yen, M.-C. & Matsumoto, J. (2012) Interannual variation of the late fall rainfall in Central Vietnam. *Journal of Climate*, 25, 392–413. Available from: https://doi.org/10.1175/JCLI-D-11-00068.1

Chen, T.-C., Tsay, J.-D., Yen, M.-C. & Matsumoto, J. (2013) The winter rainfall of Malaysia. *Journal of Climate*, 26, 936–958. Available from: https://doi.org/10.1175/JCLI-D-12-00174.1

DaSilva, N.A. & Matthews, A.J. (2021) Impact of the madden–Julian oscillation on extreme precipitation over the western maritime continent and Southeast Asia. *Quarterly Journal of the Royal Meteorological Society*, 147, 3434–3453. Available from: https://doi.org/10.1002/qj.4136

Diong, J.-Y., Xavier, P., Woolnough, S.J. & Abdullah, F.A. (2023) Equatorial Rossby waves on cold surge days and their impact on rainfall. *Quarterly Journal of the Royal Meteorological Society*, 149, 2031–2047. Available from: https://doi.org/10.1002/qj.4493

Feng, X., Yang, G.Y., Hodges, K.I. & Methven, J. (2023) Equatorial waves as useful precursors to tropical cyclone occurrence and intensification. *Nature Communications*, 14, 511. Available from: https://doi.org/10.1038/s41467-023-36055-5

Ferrett, S., Methven, J., Woolnough, S.J., Yang, G.-Y., Holloway, C.E. & Wolf, G. (2023) Hybrid dynamical–statistical forecasts of the risk of rainfall in Southeast Asia dependent on equatorial waves. *Monthly Weather Review*, 151, 2139–2152 https://journals.ametsoc.org/view/journals/mwre/151/8/MWR-D-22-0300.1.xml

Ferrett, S., Yang, G.Y., Woolnough, S.J., Methven, J., Hodges, K. & Holloway, C.E. (2020) Linking extreme precipitation in Southeast Asia to equatorial waves. *Quarterly Journal of the Royal Meteorological Society*, 146, 665–684. Available from: https://doi.org/10.1002/qj.3699

Gonzalez, P.L.M., Howard, E., Ferrett, S., Frame, T.H.A., Martínez-Alvarado, O., Methven, J. et al. (2023) Weather patterns in Southeast Asia: enhancing high-impact weather subseasonal forecast skill. *Quarterly Journal of the Royal Meteorological*

Society, 149(750), 19–39. Available from: https://doi.org/10.1002/qj.4378

Hardy, S., Methven, J., Schwendike, J., Harvey, B. & Cullen, M. (2023) Examining the dynamics of a South China Sea vortex using a balance approximation tool, weather Clim. *Dynamis*, 4, 1019–1043. Available from: https://doi.org/10.5194/wcd-4-1019-2023

Hattori, M., Mori, S. & Matsumoto, J. (2011) The cross-equatorial northerly surge over the maritime continent and its relationship to precipitation patterns. *Journal of the Meteorological Society of Japan*, 89A, 27–47. Available from: https://doi.org/10.2151/JMSJ.2011-A02

Hersbach, H., Bell, B., Berrisford, P., Hirahara, S., Horányi, A., Muñoz-Sabater, J. et al. (2020) The ERA5 global reanalysis. *Quarterly Journal of the Royal Meteorological Society*, 146, 1999–2049. Available from: https://doi.org/10.1002/qj.3803

Hodges, K.I. (1994) A general method for tracking analysis and its application to meteorological data. *Monthly Weather Review*, 122, 2573–2586. Available from: https://doi.org/10.1175/1520-0493(1994)122,2573:AGMFTA.2.0.CO;2

Hodges, K.I. (1995) Feature tracking on the unit sphere. *Monthly Weather Review*, 123, 3458–3465. Available from: https://doi.org/10.1175/1520-0493(1995)123

Hodges, K.I. (1999) Adaptive constraints for feature tracking. *Monthly Weather Review*, 127, 1362–1373. Available from: https://doi.org/10.1175/1520-0493(1999)127,1362:ACFFT.2.0.CO;2

Howard, E., Thomas, S., Frame, T.H.A., Gonzalez, P.L.M., Methven, J., Martínez-Alvarado, O. et al. (2021) Weather patterns in Southeast Asia: relationship with tropical variability and heavy precipitation. *Quarterly Journal of the Royal Meteorological Society*, 148, 747–769. Available from: https://doi.org/10.1002/qj.4227

Huffman, G.J., Bolvin, D.T., Nelkin, E.J. & Tan, J. (2020) Integrated multi-satellitE retrievals for GPM (IMERG) technical documentation. Available from: https://docserver.gesdisc.eosdis.nasa.gov/public/project/GPM/IMERG_doc.06.pdf

Isnoor, K.F., Firdianto, P.U. & Rejeki, H.A. (2019) The activity of Borneo vortex as a trigger for extreme rain in West Borneo (case study: 24th–25th January 2017). *IOP Conference Series: Earth and Environmental Science*, 303, 012061. Available from: https://doi.org/10.1088/1755-1315/303/1/012061

Jeong, J.-H., Kim, B.-M., Ho, C.-H. & Noh, Y.-H. (2008) Systematic variation in wintertime precipitation in East Asia by MJO-induced extratropical vertical motion. *Journal of Climate*, 21, 788–801.

Johnson, R. & Houze, R. (1987) *Precipitating cloud systems of the Asian monsoon*. Oxford, UK: Monsoon Meteorology, Oxford University Press, pp. 298–353.

Juneng, L., Tangang, F.T. & Reason, C.J.C. (2007) Numerical study of an extreme rainfall event during 9-11 December 2004 over the east coast of peninsular Malaysia. *Meteorology and Atmospheric Physics*, 98, 81–98.

Knapp, K.R., Kruk, M.C., Levinson, D.H., Diamond, H.J. & Neumann, C.J. (2010) The international best track archive for climate stewardship (IBTrACS): unifying tropical cyclone data. *Bulletin of the American Meteorological Society*, 91(3), 363–376. Available from: https://doi.org/10.1175/2009BAMS2755.1

Knippertz, P., Gehne, M., Kiladis, G.N., Kikuchi, K., Satheesh, A.R., Roundy, P.E. et al. (2022) The intricacies of identifying equatorial waves. *Quarterly Journal of the Royal Meteorological Society*, 148, 2814–2852. Available from: https://doi.org/10.1002/qj.4338

Koseki, S., Koh, T.-Y. & Teo, C.-K. (2014) Borneo vortex and mesoscale convective rainfall. *Atmospheric Chemistry and Physics*, 14, 4539–4562.

Latos, B., Lefort, T., Flatau, M.K., Flatau, P.J., Permana, D.S., Baranowski, D.B. et al. (2021) Equatorial waves triggering extreme rainfall and floods in southwest Sulawesi, Indonesia. *Monthly Weather Review*, 149, 1381–1401.

Liang, J., Catto, J.L., Hawcroft, M.K., Hodges, K.I., Tan, M.L. & Haywood, J.M. (2021) Climatology of Borneo vortices in the HadGEM3-GC3.1 general circulation model. *Journal of Climate*, 34, 3401–3419.

Lim, H. & Chang, C.P. (1981) A theory for midlatitude forcing of tropical motions during winter monsoons (Southeast Asia). *Journal of the Atmospheric Sciences*, 38, 2377–2392. Available from: https://doi.org/10.1175/1520-0469(1981)038,2377:ATFMFO.2.0.CO;2

Lim, S.Y., Marzin, C., Xavier, P., Chang, C.P. & Timbal, B. (2017) Impacts of boreal winter monsoon cold surges and the interaction with MJO on Southeast Asia rainfall. *Journal of Climate*, 30, 4267–4281. Available from: https://doi.org/10.1175/JCLI-D-16-0546.1

Lubis, S.W. & Jacobi, C. (2015) The modulating influence of convectively coupled equatorial waves (CCEWs) on the variability of tropical precipitation. *International Journal of Climatology*, 35, 1465–1483. Available from: https://doi.org/10.1002/joc.4069

Lubis, S.W. & Respati, M.R. (2021) Impacts of convectively coupled equatorial waves on rainfall extremes in Java. *International Journal of Climatology*, 41, 2418–2440. Available from: https://doi.org/10.1002/joc.6967

Muhammad, F.R., Lubis, S.W. & Setiawan, S. (2020) Impacts of the madden-Julian oscillation on precipitation extremes in Indonesia. *International Journal of Climatology*, 41, 1970–1984. Available from: https://doi.org/10.1002/joc.6941

Nugyen, D.Q., Renwick, J. & McGregor, J. (2016) On the presence of tropical vortices over the southeast Asian Sea–maritime continent region. *Journal of Climate*, 29, 4793–4800. Available from: doi. 10.1175/JCLI-D-14-00468.1

Ooi, S.H., Samah, A.A. & Braesicke, P. (2011) A case study of the Borneo vortex genesis and its interactions with the global circulation. *Journal of Geophysical Research*, 116, D21116. Available from: https://doi.org/10.1029/2011JD015991

Peatman, S.C., Matthews, A.J. & Stevens, D.P. (2014) Propagation of the madden–Julian oscillation through the maritime continent and scale interaction with the diurnal cycle of precipitation. *Quarterly Journal of the Royal Meteorological Society*, 140, 814–825. Available from: https://doi.org/10.1002/qj.2161

Wang, B. & Rui, H. (1990) Synoptic climatology of transient tropical intraseasonal convection anomalies: 1975-1985. *Meteorology and Atmospheric Physics*, 44, 43–61.

Wheeler, M.C. & Hendon, H.H. (2004) An all-season realtime multivariate MJO index: development of an index for monitoring and prediction. *Monthly Weather Review*, 132, 1917–1932. Available from: https://doi.org/10.1175/1520-0493(2004)132,1917:AARMMI.2.0.CO;2

Xavier, P., Rahmat, R., Cheong, W.K. & Wallace, E. (2014) Influence of madden-Julian oscillation on Southeast Asia rainfall extremes: observations and predictability. *Geophysical Research*

Letters, 41, 4406–4412. Available from: https://doi.org/10.1002/2014GL060241

Yang, G.-Y., Feng, X. & Hodges, K. (2023) Seasonal and interannual variation of equatorial waves in ERA5 and GloSea5. *Quarterly Journal of the Royal Meteorological Society*, 149(752), 1109–1134. Available from: https://doi.org/10.1002/qj.4460

Yang, G.-Y., Ferrett, S., Woolnough, S., Methven, J. & Holloway, C. (2021) Real-time identification of equatorial waves and evaluation of waves in global forecasts. *Weather and Forecasting*, 36(1), 171–193. Available from: https://doi.org/10.1175/WAF-D-20-0144.1

Yang, G.-Y., Hoskins, B. & Slingo, J. (2003) Convectively coupled equatorial waves: a new methodology for identifying wave structures in observational data. *Journal of the Atmospheric Sciences*, 60, 1637–1654. Available from: https://doi.org/10.1175/1520-0469%282003%29060%3C1637%3ACCEWAN%3E2.0.CO%3B2

SUPPORTING INFORMATION

Additional supporting information can be found online in the Supporting Information section at the end of this article.

How to cite this article: Crook, J., Hardy, S., Methven, J., Schwendike, J., Yik, D.J. & Yang, G.-Y. (2024) The structure of Borneo vortices and their relationship with cold surges, the Madden–Julian oscillation and equatorial waves. *Quarterly Journal of the Royal Meteorological Society*, 1–25. Available from: https://doi.org/10.1002/qj.4905